AGU PUBLICATIONS

JGR

Journal of Geophysical Research: Space Physics

RESEARCH ARTICLE
10.1002/2014JA020281

Special Section:
New perspectives on Earth's radiation belt regions from the prime mission of the Van Allen Probes

Weak kinetic Alfvén waves turbulence during the 14 November 2012 geomagnetic storm: Van Allen Probes observations

Pablo. S. Moya[1,2,3], Víctor A. Pinto[4], Adolfo F. Viñas[1], David G. Sibeck[5], William S. Kurth[6], George B. Hospodarsky[6], and John R. Wygant[7]

[1]Geospace Physics Laboratory, NASA Goddard Space Flight Center, Greenbelt, Maryland, USA, [2]Department of Physics, Catholic University of America, Washington, District of Columbia, USA, [3]Departmento de Física, Facultad de Ciencias, Universidad de Chile, Santiago, Chile, [4]Department of Atmospheric and Oceanic Sciences, University of California, Los Angeles, California, USA, [5]Space Weather Laboratory, NASA Goddard Space Flight Center, Greenbelt, Maryland, USA, [6]Department of Physics and Astronomy, University of Iowa, Iowa City, Iowa, USA, [7]School of Physics and Astronomy, University of Minnesota, Minneapolis, Minnesota, USA

Key Points:

- Observation of striking magnetic fluctuations during the 14 November 2012 magnetic storm
- Spectral analysis suggests the presence of kinetic Alfvén waves turbulence
- The interpretation is consistent with Vlasov linear theory analysis

Correspondence to:
P. S. Moya,
pablo.s.moyafuentes@nasa.gov

Citation:
Moya, P. S., V. A. Pinto, A. F. Viñas, D. G. Sibeck, W. S. Kurth, G. B. Hospodarsky, and J. R. Wygant (2015), Weak kinetic Alfvén waves turbulence during the 14 November 2012 geomagnetic storm: Van Allen Probes observations, *J. Geophys. Res. Space Physics*, *120*, doi:10.1002/2014JA020281.

Received 10 JUN 2014
Accepted 23 JUN 2015
Accepted article online 29 JUN 2015

Abstract In the dawn sector, $L \sim 5.5$ and MLT $\sim 4-7$, from 01:30 to 06:00 UT during the 14 November 2012 geomagnetic storm, both Van Allen Probes observed an alternating sequence of locally quiet and disturbed intervals with two strikingly different power fluctuation levels and magnetic field orientations: either small ($\sim 10^{-2}$ nT^2) total power with strong GSM B_x and weak B_y or large (~ 10 nT^2) total power with weak B_x and strong B_y and B_z components. During both kinds of intervals the fluctuations occur in the vicinity of the local ion gyrofrequencies (0.01–10 Hz) in the spacecraft frame, propagate oblique to the magnetic field, ($\theta \sim 60°$), and have magnetic compressibility $C = |\delta B_\parallel|/|\delta B_\perp| \sim 1$, where $\delta B_\parallel$ ($\delta B_\perp$) are the average amplitudes of the fluctuations parallel (perpendicular) to the mean field. Electric field fluctuations are present whenever the magnetic field is disturbed, and large electric field fluctuations follow the same pattern for quiet and disturbed intervals. Magnetic frequency power spectra at both spacecraft correspond to steep power laws $\sim f^{-\alpha}$ with $4 < \alpha < 5$ for $f \lesssim 2$ Hz, and $1.1 < \alpha < 1.7$ for $f \gtrsim 2$ Hz, spectral profiles that are consistent with weak kinetic Alfvén wave (KAW) turbulence. Electric power is larger than magnetic power for all frequencies above 0.1 Hz, and the ratio increases with increasing frequency. Vlasov linear analysis is consistent with the presence of compressive KAW with $k_\perp \rho_i \lesssim 1$, right-handed polarization and positive magnetic helicity, in the plasma frame, considering a multiion plasma. All these results suggest the presence of weak KAW turbulence which dissipates the energy associated with the intermittent sudden changes in the magnetic field during the main phase of the storm.

1. Introduction

Geomagnetic storms are probably the most important processes associated with solar-terrestrial interaction [*Gonzalez et al.*, 1994]. Wave-particle interactions with electromagnetic waves are believed to play an important role regulating the radiation belts dynamics during storms. Despite decades of intense theoretical and observational studies, a definitive framework for the wave-particle interactions and the resulting effects in the magnetospheric dynamics remains an open problem. The recent launch of the Van Allen Probes mission [*Mauk et al.*, 2012; *Stratton et al.*, 2013] opened a variety of new opportunities for understanding the dynamics of the Earth's radiation belts. The onboard plasma, magnetic field, and electric field instruments offer both high time resolution and high-quality data for precise wave analysis. Already obtained data sets can be used to identify the basic characteristic features of electric and magnetic fluctuations and the corresponding behavior of the plasma, marking a key step toward understanding wave-particle interaction, in particular, for waves in the frequency range of the particles gyrofrequencies such as electromagnetic ion cyclotron (EMIC) waves [*Kennel and Petschek*, 1966; *Thorne and Kennel*, 1971; *Viñas et al.*, 1984; *Gomberoff and Elgueta*, 1991; *Gary*, 1992; *Gomberoff and Valdivia*, 2003] or kinetic Alfvén waves (KAWs) [*Hasegawa*, 1976; *Gary*, 1986; *Hollweg*, 1999].

EMIC waves have been observed at low altitudes [*Young et al.*, 1981; *Mauk*, 1982; *Lee et al.*, 2012] and high latitudes [*Erlandson et al.*, 1990; *Mursula et al.*, 1994] and at different distances from the Earth; the ionosphere [*Iyemori and Hayashi*, 1989; *Bräysy et al.*, 1998], the plasmapause—ring current boundary [*LaBelle et al.*, 1988], at low L shell [*Erlandson and Ukhorskiy*, 2001] and up to more than 10 R_E [*Anderson et al.*, 1992a, 1992b; *Zhang et al.*, 2010; *Min et al.*, 2012], and at different magnetic local time [*Keika et al.*, 2013a]. EMIC waves are left-handed polarized waves, have frequencies near and below the local ion gyrofrequencies (such as H^+, He^+, and O^+ ions), and in the absence of relative drift between species are limited by stop bands bounded by the ion gyrofrequencies [*Gomberoff and Elgueta*, 1991; *Thorne and Horne*, 1994; *Gomberoff and Valdivia*, 2003]. These waves can propagate parallel [*Cornwall*, 1965; *Anderson et al.*, 1996; *Keika et al.*, 2013a] or oblique [*Thorne and Horne*, 1992; *Khazanov et al.*, 2007] to the mean magnetic field and are produced by ion-cyclotron resonant absorption of the free energy stored in anisotropic ion populations [see, e.g., *Gamayunov et al.*, 2009; *Khazanov*, 2011]. Observations and theoretical models have shown that EMIC waves play an important role in the evolution of the ring current during the main phase of storms [*Thorne and Kennel*, 1971; *Hamilton et al.*, 1988; *Thorne and Horne*, 1994, 1997; *Daglis*, 1997; *Daglis et al.*, 1999; *Keika et al.*, 2013b], in electron precipitation due to pitch angle scattering [*Thorne and Horne*, 1992; *Summers and Thorne*, 2003; *Khazanov et al.*, 2007; *Khazanov*, 2011; *Omura and Zhao*, 2013], and in ionosphere-magnetosphere coupling [*Gamayunov et al.*, 2009].

On the other hand, KAWs have been observed at the magnetopause [*Johnson et al.*, 2001; *Chaston et al.*, 2005], in the plasma sheet [*Wygant et al.*, 2002; *Chaston et al.*, 2012], at geostationary orbit [*Kloecker et al.*, 1985; *Perraut et al.*, 2000], and in the inner magnetosphere [*Huang et al.*, 1997; *Chaston et al.*, 2006, 2014]. KAWs have frequencies in the proton gyrofrequency range, have quasi-perpendicular wave normal angles [*Cornwall*, 1965] and require plasma conditions such that the wavelength is similar to the ions' gyroradius ($k_\perp \rho_i \sim 1$) [*Hollweg*, 1999; *Voitenko and Goossens*, 2006; *Lysak*, 2008]. One of the key signatures that distinguishes the KAW mode from EMIC waves is the polarization. Unlike EMIC waves, in the plasma frame KAWs are right-hand polarized, result that has been obtained using fluids [*Hollweg*, 1999] and kinetic models [*Gary*, 1986]. Thus, even though they can resonate with ions under certain conditions, KAW wave-particle interactions are, in general, nonresonant with ions and resonant with electrons. As studied by *Gary* [1986], the shift from left- to right-handed polarization is strongly dependent on the local plasma β, meaning that higher β allows the plasma to develop KAW at lower propagation angles with respect to the mean field. KAWs are typically magnetically compressive and have large parallel electric fields. Another important characteristics of the KAW mode is the large fluctuating electric field compared with the case of EMIC waves. This has been indicated from theory [*Gary*, 1986; *Hollweg*, 1999; *Voitenko and Goossens*, 2006] and observations [see, e.g., *Wygant et al.*, 2002; *Chaston et al.*, 2014]. In particular, the ratio between electric and magnetic field fluctuations $\delta E/\delta B$ is an important signature to distinguish between ion-cyclotron waves and kinetic Alfvén waves. The former mode exhibits $\delta E/\delta B$ of the order of the local Alfvén speed, and in the case of the later $\delta E/\delta B$ is usually larger than the local Alfvén speed and increases with increasing frequency or $k_\perp \rho_i$ value. Observations have shown that KAWs play an important role in the ion demagnetization and heating in the inner magnetosphere [*Chaston et al.*, 2014], in the ionospheric O^+ outflow due to reconnection during substorms [*Chaston et al.*, 2005], in auroral electron acceleration [*Hasegawa*, 1976; *Chaston et al.*, 2006], and in electron energization at the plasma sheet boundary layer [*Kloecker et al.*, 1985; *Wygant et al.*, 2002]. Also, theoretical results have shown that KAW may be relevant for the ion transport [*Hasegawa and Mima*, 1978; *Lee et al.*, 1994] and heating [*Johnson et al.*, 2001; *Johnson and Cheng*, 2001] at the dayside magnetopause.

It is well known that like KAWs, Magnetosonic waves (MSW) are also right-hand polarized and magnetically compressive waves. The distinction between MSWs and KAWs in space plasma observations is a current hot topic in the community. Both modes can coexist and share some similar properties in the observations. However, magnetic compressibility and $\delta E/\delta B$ ratio are quite different for the two modes. In the spacecraft frame MSWs have approximately constant magnetic compressibility and a monotonically increasing $\delta E/\delta B$ ratio frequency spectrum (the frequencies can go up to the electron cyclotron frequency when MSW transform to whistler waves, see, for example, *Stringer* [1963], *Santolík et al.* [2002], *Mourenas et al.* [2013]), whereas KAWs have a complex compressibility frequency spectrum and exhibit a $\delta E/\delta B$ ratio spectrum with a local maximum at a given frequency (depending on the plasma parameters), which then decreases for larger frequencies [*Salem et al.*, 2012].

To characterize the waves and distinguish between several possible wave modes (EMIC, KAW, or MSW, among others), the wave normal propagation direction **k** is perhaps the most important spectral physical quantity required. There have been various studies of wave normal propagation direction and wave properties which have focused on the reliability of the identification of these spectral properties from spacecraft observations in the magnetosphere [see, e.g., *Fowler et al.*, 1967; *Rankin and Kurtz*, 1970; *Means*, 1972; *Anderson et al.*, 1996;

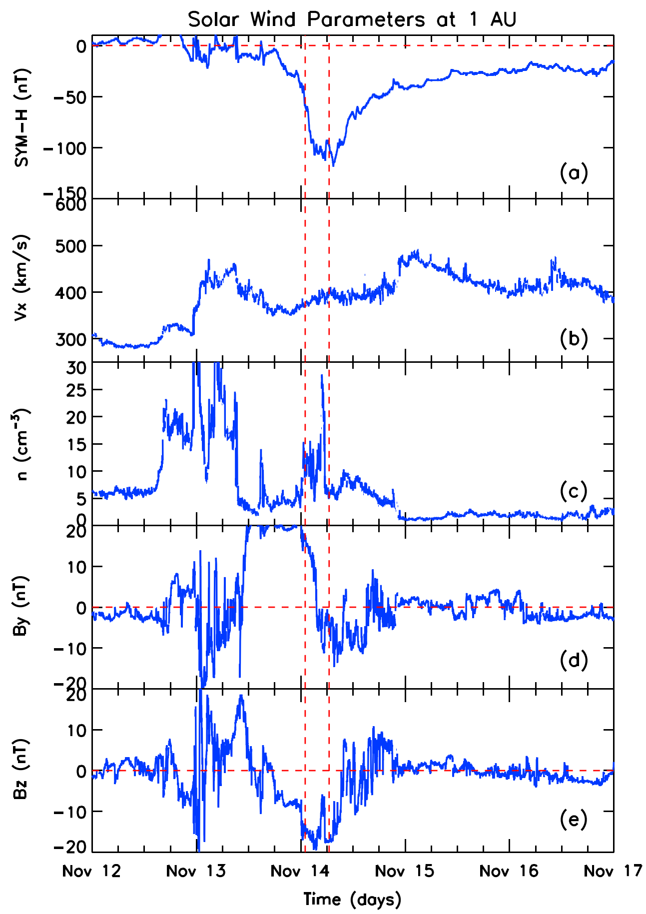

Figure 1. Summary plots from 12 to 16 November 2012 for the geomagnetic storm from OMNI data. Vertical red lines mark the studied time interval between 01:30 and 06:00 UT 14 November 2012. (a) *SYM-H* index. (b) Absolute value of solar wind *Vx* (GSE). (c) Solar wind density. (d) IMF B_y GSE component. (e) IMF B_z GSE component.

Denton et al., 1996]. In this article we report results from an observational and theoretical study of the electromagnetic fluctuations associated with the 14 November geomagnetic storm using high-resolution data from the Van Allen Probes mission. In the next section we describe the topological characteristics of the electric and magnetic fields during the storm, and obtain basic characteristics (such as wave normal propagation direction, compressibility, and power and helicity frequency spectrum) associated with the electromagnetic fluctuations. In section 3 we compute the linear Vlasov eigenfrequencies and eigenvectors and obtain theoretical expressions for spectral properties as a function of wave number. We compare the spectra as a function of frequency in the spacecraft frame with the theoretical spectra for the corresponding conditions. Finally, in section 4 we summarize and discuss our results.

2. Instrumentation and Data Analysis

The 14 November 2012 geomagnetic storm was one of the first measured by the Van Allen Probes, whose measurements show an unusual set of striking magnetic fluctuations rarely seen before (see discussion below). This particular storm was moderate with a minimum *SYM-H* index of −118 nT at 07:30 UT. The storm was caused by a shock with an Interplanetary Coronal Mass Ejection (ICME) that arrived to the Earth at about 10 UT on 12 November 2012. In Figure 1 we show 1 AU solar wind conditions between 00:00 (UT) 12 November 2012 and 23:59(UT) 14 November 2012. The figure exhibits the increase in speed (Figure 1b) and density (Figure 1c) expected at the arrival of the ICME, as well as the decrease in density during the recovery phase. In addition, Figures 1d and 1e show a large southward B_z (~ -15 nT) IMF and IMF B_y rotating from positive to negative values during the main phase of the storm. The time of interest for our study is between 01:30 UT and 06:00 UT on 14 November 2012, which corresponds to almost the entire main phase of the storm and includes the

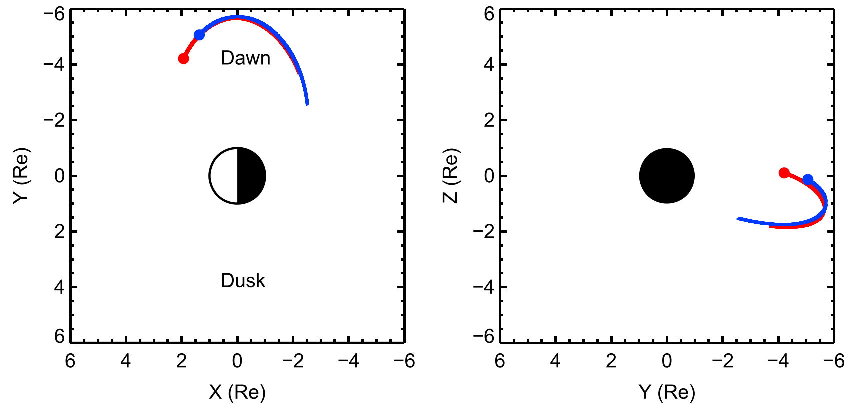

Figure 2. Position of the Van Allen Probes during the studied interval. (left) GSM equatorial plane. (right) GSM $X = 0$ plane. Red and blue curves correspond to probes A and B, respectively, and the circles correspond to spacecraft positions at 06:00 UT.

largest magnetic fluctuations. During this time interval the Van Allen Probes were in the dawn sector moving from the nightside to the dayside at low magnetic latitude as shown in Figure 2, L shell between 4 and 6, and MLT between 4 and 7 (not shown).

We use Electric and Magnetic Field Instrument Suite and Integrated Science (EMFISIS) magnetometer and waves instrument, and Electric Field and Waves (EFW) instrument observations from the Van Allen Probes. From the EMFISIS instrument we considered data from the flux gate Magnetometer (MAG) that provide magnetic field observations with a time resolution of 64 magnetic vectors per second [*Kletzing et al.*, 2013]. From the EFW instrument, we considered 32 vectors per second despun electric field measurements in modified-GSE (MGSE) coordinates [*Wygant et al.*, 2013]. EMFISIS also includes a Waves instrument that measures three-component electric and magnetic field measurements of waves from ~2 Hz to 12 kHz, and single single electric field component of waves from 10 kHz to 400 kHz (using search coils and EFW high-frequency electric field sensors) from which the electron density can be determined [*Kurth et al.*, 2015].

2.1. Magnetic Field Observations

During the interval of interest we observe abrupt changes in the magnetic field, that seem like discontinuities between two different magnetic field configurations. Figure 3 shows intermittency between relatively long intervals (for example, 02:06–02:45 UT or 02:55–03:35 UT), with strong GSM B_x and weak B_y magnetic fields, and short disturbed intervals (for example, 01:55–02:06 UT, 02:45–02:55 UT, or 04:40–04:55 UT), with weak B_x and strong B_y and B_z components. This intermittency is observed by both spacecraft (red and blue lines in the figure) with a small delay of about 5 min between probes B and A measurements. In Figures 3h–3j we show projections of the observed magnetic field sudden changes in the GSM $Y = 0$ plane, during three of the disturbed intervals. From the diagrams we clearly observe abrupt transitions between relatively stretched magnetic field configurations right before the disturbed intervals (blue arrows), sudden jumps to a more dipolar field configuration (red arrows), and then restorations of the field to the initial configuration (green arrows). These changes in the magnetic field configuration are accompanied by very unusual disturbances in the measured electron density n_e (obtained from the frequency of the upper hybrid and plasma lines and the magnitude of the measured magnetic field), showing sharp density dropouts, with densities atypically low for this region, as seen for both spacecraft in Figure 3g. It is important to mention that the particular conditions of the event made the determination of the upper hybrid line and/or plasma line cutoff challenging (not shown). Thus, in this case the method used (described in detail by *Kurth et al.* [2015]) provides only an upper limit to the local plasma frequency and therefore an upper limit to the local electron density.

There is currently an interesting debate in the community regarding the nature of the magnetic field observations with two main proposed explanations. One interpretation associates the magnetic fluctuations with the passages through the boundary between closed and open (stretched) magnetic field lines. Due to the storm activity, this boundary layer moves back and forth across the spacecraft. Based on global MHD simulations, this interpretation is consistent with the density dropouts shown in Figure 3g (the density is expected to be higher in closed magnetic field configuration and smaller during intervals with strong B_y magnetic field) and the observed *SYM-H* index profile [*Glocer et al.*, 2013]. A second interpretation explains the magnetic fluctuations

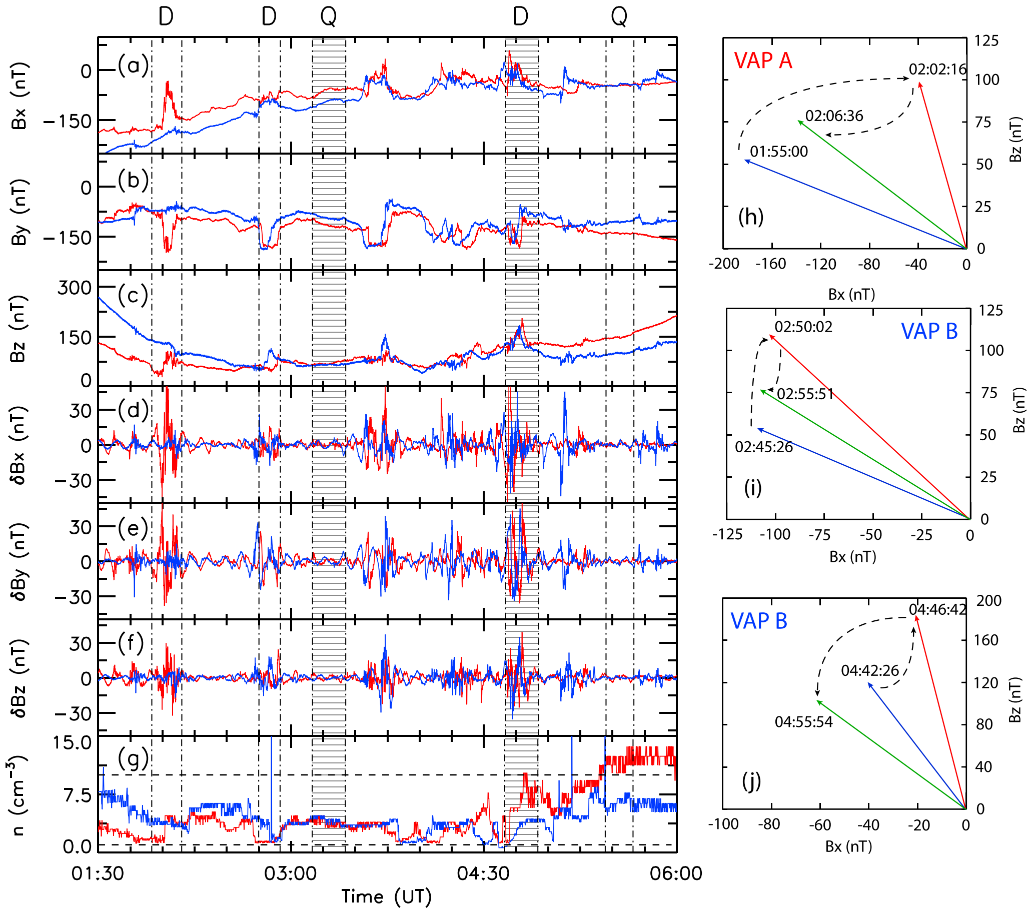

Figure 3. (left) Van Allen Probes magnetic field and electron density data from 01:30 to 06:00 UT during the 14 November 2012 geomagnetic storm in GSM coordinates. (a) B_x. (b) B_y. (c) B_z. (d) B_x fluctuations. (e) B_y fluctuations. (f) B_z fluctuations. (g) electron density obtained from the upper hybrid and plasma lines. Red and blue lines correspond to probes A and B, respectively. Selected quiet (Q) and disturbed (D) intervals are marked with dash-dotted vertical lines and gray areas. Gray regions also correspond to the intervals studied in detail in section 2.2. (right) Projections of the local magnetic field in the GSM $Y = 0$ during the disturbed interval at (h) 01:55–02:06 UT and at (i) 02:45–02:55 UT and 04:40–04:55 UT, respectively.

in terms of magnetic flux ropes sequentially generated moving earthward from reconnection sites in the tail current sheet [*Hwang et al.*, 2015]. Under this interpretation each magnetic-disturbed interval corresponds to an encounter with a moving magnetic flux bundle that contains a low-density population by the spacecraft. This picture is consistent with the abrupt changes in the magnetic field orientation, the intermittent activity, and the reduced plasma density during these intervals. Here we address the fluctuations themselves and their principal characteristics without discriminating between the models for these global magnetic field configurations and their causes.

To focus upon the magnetic field fluctuations and remove the large-scale gradients of the magnetic field, we applied a high pass filter cutting frequencies lower than 2 mHz, using the Fast Fourier Transform (FFT) technique. From these fluctuations (Figures 3d to 3f) we observe important differences between quiet and disturbed intervals when B_y is large. It is clear that both spacecraft observe significant (amplitudes greater than 15 nT) fluctuations mainly during disturbed intervals. We used an FFT algorithm to compute a one-dimensional power spectral density (PSD) matrix $\mathbf{P} =< \tilde{B}_i \tilde{B}_j^* >$, where $\tilde{\mathbf{B}}$ is the complex magnetic field in the Fourier frequency domain, for overlapping intersecting intervals with 2048 points (32 s long), in the spacecraft frame. The trace of **P** (the frequency power spectrum) is shown in Figures 4a and 4b for probes A and B, respectively. The figure shows that most of the power occurs at frequencies below the H^+, He^+, and O^+ local gyrofrequencies, consistent with EMIC waves properties. However, the frequency range is not banded as expected for EMIC waves. By contrast we observe a broadband spectrum with substantial power even for

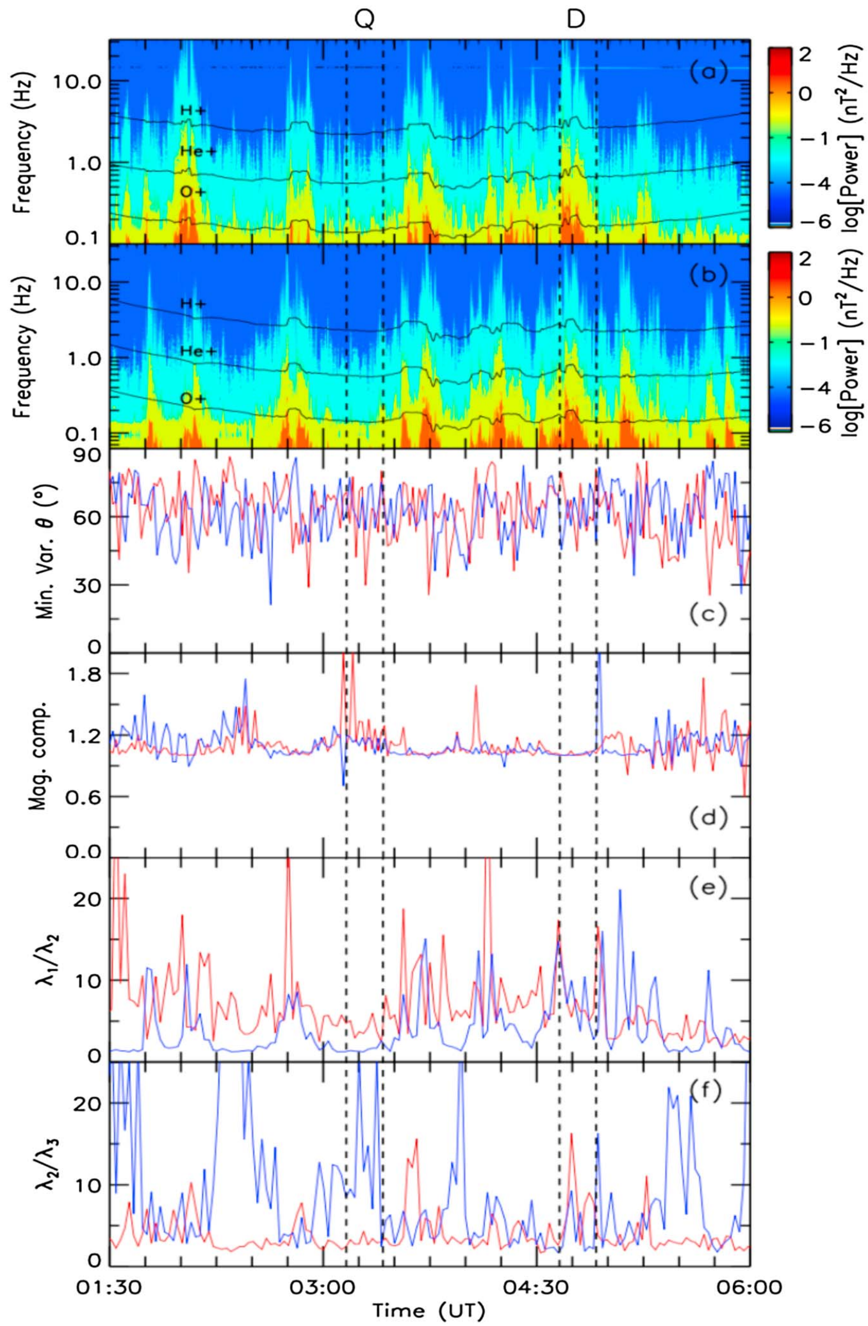

Figure 4. Spectrogram of waves observed by (a) probe A and (b) probe B from 01:30 to 06:00 UT, showing gyrofrequencies of H^+, He^+, and O^+ ions. The 14.5 Hz signal arises from an aliased heater line and was not included in the calculations. (c) Angle between MVA direction of propagation of the waves and local magnetic mean field during the same time interval as in Figures 4a and 4b. Here we remove the minimum variance ambiguity showing only acute angles, meaning that a given angle θ is representative of $\pm\theta$. (d) Magnetic compressibility of the fluctuations during the same time interval. Minimum variance analysis eigenvalues ratios, (e) largest to medium eigenvalues (λ_1/λ_2) ratio, (f) medium to smallest eigenvalues (λ_2/λ_3) ratio. Red and blue lines correspond to probes A and B, respectively. Selected quiet (Q) and disturbed (D) intervals are marked with dash-dotted vertical lines.

frequencies above H^+ gyrofrequency at both spacecraft, particularly during disturbed intervals. Thus, instead of EMIC wave spectra, the observations are more consistent with the presence of a process that results in a broadband spectrum of fluctuations. Comparing the quiet (Q) and disturbed (D) intervals marked in Figure 4 we observe much more activity during disturbed intervals. Thus, whatever the physical process producing the observed magnetic abrupt changes, that process should be related with the observed magnetic fluctuations and their intermittency. The ∼3 order of magnitude difference between the fluctuations power during quiet and disturbed intervals indicate that the amplitude of the fluctuations is closely related with the changes in the magnetic field configuration. We will return to this point later once we have studied the event more in depth.

To extract more information about the observed spectra of magnetic fluctuations we performed a Minimum Variance Analysis (MVA) [*Sonnerup and Cahill*, 1967; *Sonnerup and Scheible*, 1998] to obtain the direction of propagation of the fluctuations for both spacecraft. Within each 32 s interval, for each spacecraft we computed the mean magnetic field and then an eigenvalues and eigenvectors calculation to obtain a minimum variance direction, from which we obtained the angle of propagation θ of the fluctuations relative to the mean field. We also computed the magnetic compressibility of the fluctuations, defined as $C = |\delta B_{\parallel}|/|\delta B_{\perp}|$, where $\delta B_{\parallel}$, $\delta B_{\perp}$ are the average amplitudes of the fluctuations parallel and perpendicular to the mean field. We found that throughout most of the time interval the waves are highly oblique at both spacecraft, propagating at about 60°with respect to the mean field direction (with an ambiguity in the sign), and the magnetic compressibility is of order 1 as shown in Figures 4c and 4d. We further observe that the magnetic compressibility is slightly smaller and less fluctuating usually during disturbed intervals than during quiet times. The reliability of the minimum variance analysis can be determined by the ratio between the obtained eigenvalues. In Figure 4 we also present the largest to medium eigenvalues (λ_1/λ_2) ratio (Figure 4e), and the medium to smallest eigenvalues (λ_2/λ_3) ratio (Figure 4f). Both panels show reasonable eigenvalue ratios, ensuring a well-defined minimum variance direction. In summary we observe broadband spectra of highly oblique and compressive magnetic fluctuations, with most of the power at frequencies below the local ion gyrofrequencies.

2.2. Comparison of the Spectral Characteristics During Quiet and Disturbed Periods

To further characterize the magnetic fluctuations and the differences between disturbed and quiet intervals, we selected three disturbed and two quiet short intervals of 8 to 15 min duration which correspond to the marked intervals between dash-dotted lines and gray regions in Figure 3. We studied the associated propagation and spectral characteristics of the fluctuations during each interval and compared spectral properties of the magnetic perturbations during quiet and disturbed time intervals. Figure 5 compares a quiet interval between 03:10 and 03:25 UT (left) and a disturbed interval between 04:40 and 04:55 UT (right), both intervals marked in gray in Figure 3. Note that the spectral characteristics are similar for both intervals and for both spacecraft (red and blue lines), and the main difference between quiet and disturbed intervals is in the level of the amplitudes of the fluctuations, which is consistent with the dynamic spectrogram shown in Figure 4.

Figures 5a (left) and 5a (right) present the frequency power spectrum for frequencies between 2 mHz and 10 Hz. We observe that for both spacecraft the frequency power spectra correspond to power laws frequency spectra $f^{-\alpha}$ with $\alpha \sim 4.6$ for the disturbed interval, and to $\alpha \sim 4.2$ for the quiet interval, both steeper than the characteristic Kolmogorov spectrum $f^{-5/3}$ for turbulence in the inertial range. The quiet interval also presents a spectral break at about 3 Hz (we will return to this later). This kind of power law spectra indicates electromagnetic fluctuations in the dissipation range for frequencies above the inertial range (Kolmogorov spectrum) in which large-scale nonlinear wave-wave interactions dominate, and it is associated with energy dissipation due to wave-particle interactions and temporal and spatial scales on the order of those kinetic characteristics of the plasma, such as gyrofrequency, inertial length, and gyroradius. In this particular case the observed broadband turbulent spectra of compressive and quasi-perpendicular fluctuations, with a steep power spectrum $\sim f^{-4}$ for frequencies near/below the ions' gyrofrequency (represented with vertical lines in Figure 5) is consistent with KAW turbulence in the weakly dispersive range or weak kinetic Alfvén waves turbulence, which corresponds to the intermediate frequency range above the inertial range and below $k_{\perp}\rho_i \sim 1$ and the fully developed KAW turbulence at subkinetic ion scales [*Voitenko and De Keyser*, 2011]. We observe a similar behavior during all selected intervals, with or without a spectral break separating a steep spectrum for lower frequencies and a flatter spectrum for higher frequencies. Table 1 presents a summary of the average spectral properties for each selected interval. In all cases the spectral break occurs at about 2 and 3 Hz, very close to the local proton gyrofrequency (not shown), in line with the description of the KAW turbulence with two

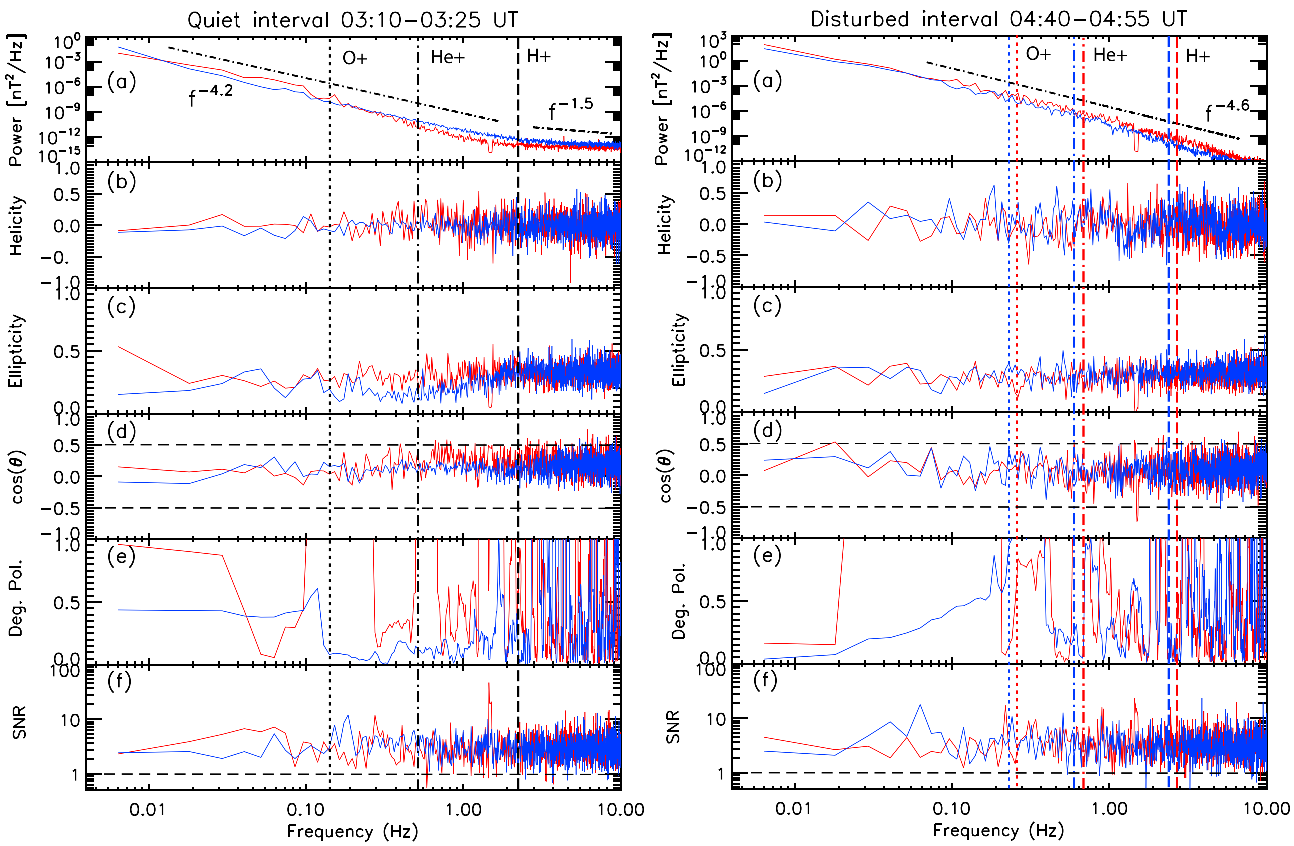

Figure 5. Spectral properties (left) from quiet interval between 03:10 and 03:25 UT and (right) from disturbed interval between 04:40 and 04:55 UT as a function of frequency. From top to bottom, (a) frequency power spectrum, (b) reduced magnetic helicity, (c) wave ellipticity, (d) cosine of the angle of polarization, (e) degree of polarization, and (f) signal to noise ratio. Red and blue curves represent spacecraft A and B calculations. In Figure 5 (right) vertical lines represent local ion gyrofrequencies for both probes. In Figure 5 (left) red and blue vertical lines represent local ion gyrofrequencies for probes A and B, respectively. Spikes at 1.5 Hz in red curves are remnants of a notch filter used to remove a signal related to coupling with other instruments on board.

different spectral slopes above or below the characteristic kinetic space and timescales of the plasma. [*Voitenko and De Keyser*, 2011].

During quiet intervals the total power of the fluctuations P_{tot} is of the order of 10^{-3} to 10^{-2} nT^2. During disturbed intervals, the total power P_{tot} is of order 10 nT^2, both results consistent with previous descriptions of disturbed and quiet intervals, in terms of more or less fluctuations amplitude, based only on the properties of the magnetic field in real space. For all intervals and both spacecraft the minimum variance angle and compressibility are similar, but the compressibility standard deviation is much higher for disturbed periods, which may indicate the presence of more field-aligned perturbations (see Table 1) or the coexistence of small background perturbations and the turbulent spectrum when the spacecraft are not observing the sudden

Table 1. Average Spectral Properties From Selected Intervals[a]

		Probe A				Probe B			
Type	Interval	α	P_{tot} (nT^2)	θ (deg)	C	α	P_{tot} (nT^2)	θ (deg)	C
D	01:55–02:06	4.6	32.41	61.3 ± 19.1	1.002 ± 0.016	4.9, 1.5	0.06	52.8 ± 20.7	1.042 ± 0.343
D	02:45–02:55	4.9, 1.7	3.56	56.27 ± 18.5	1.018 ± 0.038	4.6	0.93	67.46 ± 17.2	1.007 ± 0.113
Q[a]	03:10–03:25	4.2, 1.5	0.01	60.6 ± 20.2	1.259 ± 0.523	4.2, 1.5	0.04	64.9 ± 19.8	1.055 ± 0.571
D[a]	04:40–04:55	4.6	10.34	62.8 ± 20.0	1.010 ± 0.022	4.6	11.51	63.1 ± 19.9	1.002 ± 0.067
Q	05:27–05:40	4.3, 1.1	0.004	63.3 ± 21.2	1.112 ± 0.889	4.3, 1.1	0.007	53.8 ± 21.3	0.892 ± 0.383

[a]Detailed polarization parameters for this interval are shown in Figure 5.

changes in the magnetic field. Nevertheless, the weak KAW turbulence interpretation is consistent within all the intervals but with most of the magnetic power during disturbed intervals. Thus, we can conclude that the presence of large-amplitude fluctuations is mainly due to a local process associated with the magnetic field abrupt changes. However, with the available observations it is not clear what is the exact driver of the fluctuations. Based on the properties of KAWs, and the corresponding spectral profile of the power of the fluctuation in both quiet and disturbed intervals, our interpretation is that the fluctuations driver is the magnetic energy associated with the abrupt changes in the magnetic field configuration, and the broadband structure of the spectra is due to a turbulent cascade. Our interpretation is consistent with the mentioned explanation by *Glocer et al.* [2013] in which the fluctuations are related with a moving boundary between closed and open field lines, and also with the explanation by *Hwang et al.* [2015], in which the fluctuations are associated to the passage of magnetic flux ropes coming from the tail, providing the observed magnetic field sudden changes.

While our results suggest the presence of a spectrum of quasi-perpendicular weak kinetic Alfvén wave turbulence (i.e., nonlinear processes and coupling between waves) the presence of KAW modes can be further quantified by using spectral analysis methods such as the Stokes polarization parameters [*Fowler et al.*, 1967; *Rankin and Kurtz*, 1970; *Means*, 1972]. From this calculation we can estimate the characteristic variance ellipse from the PSD matrix, such as the reduced magnetic helicity and the wave ellipticity, among other polarization quantities [*Fowler et al.*, 1967; *Rankin and Kurtz*, 1970; *Means*, 1972]. Figures 5b – 5d and 5f show magnetic helicity, wave ellipticity, the cosine of the angle of polarization, and degree of polarization, all as a function of the frequency, for each spacecraft (red and blue lines) for the selected quiet and disturbed intervals (Figures 5, left and 5, right). The figure shows that this analysis is in agreement with the MVA results for the real fluctuations, in that the angle of polarization (between the mean magnetic field and the major axis of the polarization ellipse) computed in the frequency domain is highly oblique throughout most of the frequency range, in particular, for frequencies below 1 Hz, for both spacecraft and for both quiet and disturbed intervals. In comparison with the minimum variance direction presented in Figure 4c, in both intervals the cosine of the polarization angle spectra is roughly bounded by $\cos(\pm 60°) = \pm 0.5$, consistent with the results obtained in real space. For low frequencies the ellipticity is small and indicates the possible presence of linearly polarized waves, but increases for higher frequencies showing the presence of elliptically polarized waves. The magnetic helicity and degree of polarization spectra are quite noisy. The helicity does not exhibit a preferential sign and the degree of polarization fluctuates between frequency ranges with high or small polarized power. Thus, we can not draw further conclusions about the topological handedness of the waves, the sense of polarization of the waves in the spacecraft frame, or the total amount of polarized power observed during quiet or disturbed subintervals. However, the signal-to-noise ratio (SNR) shown in Figure 5f is greater than 1 in almost all the intervals studied with an average of SNR ~ 3, indicating that during the time of interest the power in the elliptical plane of the waves is greater than the noise or other kind of perturbations. This moderate SNR value is consistent with the observed power law frequency spectrum and noisy helicity spectrum. In summary, our results are consistent with the presence of a turbulent spectrum of highly oblique compressional waves such as KAW but the spectral analysis using only magnetic field data is not clear enough to be conclusive.

Specific information about the polarization properties of fluctuations can be obtained using hodograms; i.e., plots showing the time dependence of two different components of the fields over time intervals short enough to observe the waveforms and isolate a few wave cycles. Figure 6 show waveforms and hodograms for short intervals during the selected disturbed (04:40 – 04:55 UT) interval. As our observations contain waves with frequencies ranging over several orders of magnitude, we use a band-pass filter to show the waveforms and hodograms for two frequency ranges: between 0.1 and 1.0 Hz (Figure 6, top), and f between 1.0 and 10 Hz (Figure 6, bottom), to show the properties of the higher frequency range of the spectrum. Using minimum variance analysis, we obtained the minimum variance direction, the ratio of the maximum, intermediate, and minimum variance directions, and the rotation of the magnetic field coordinates from GSM to Minimum Variance (MV) coordinates. We observe that there is a clear highly oblique minimum variance direction in both frequency ranges represented by reasonable eigenvalues ratios, both consistent with the results shown in Figures 4e and 4f. In both cases there is a clear polarization plane represented in the hodograms between the maximum (B_1)and intermediate (B_2) variance magnetic field coordinates. From the hodograms we observe that both frequency ranges seem to exhibit elliptical polarization in the spacecraft frame. However, due to the broadband nature of the fluctuations, each 10 s or 1 s interval includes cycles for a broad range of frequencies, so it is not possible to ensure that the hodograms represent single isolated wave periods. In addition, because in plasma physics the sense of polarization is defined in relation to the mean magnetic field and not

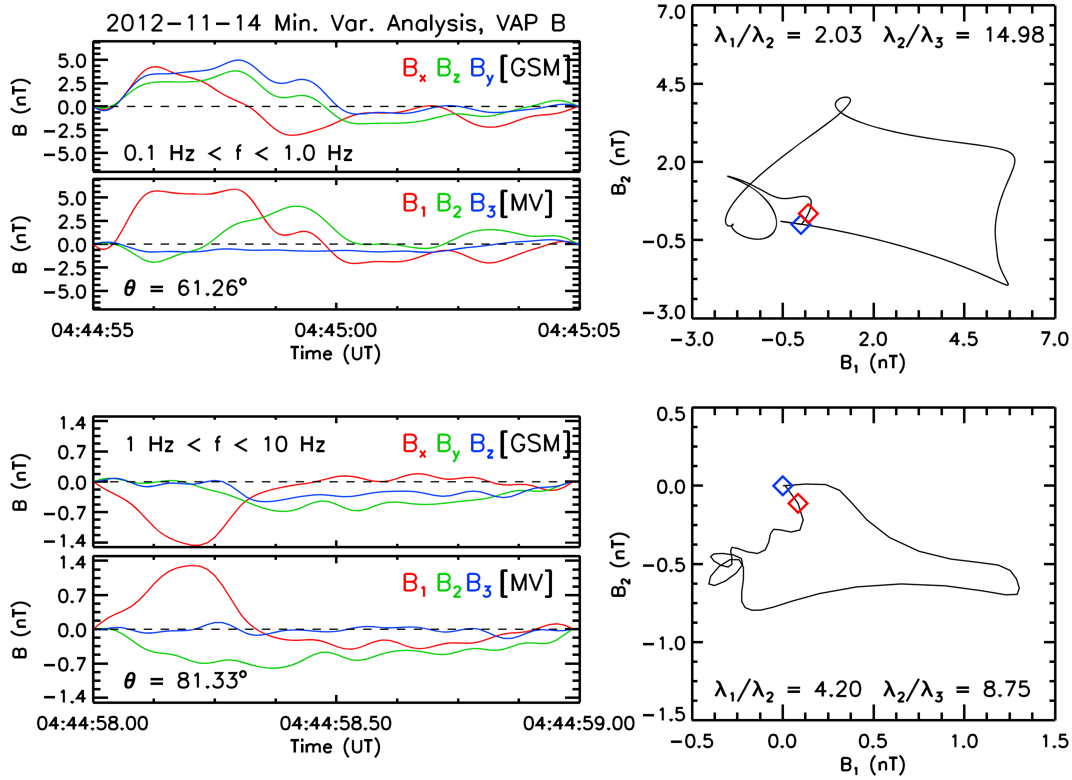

Figure 6. Hodograms for magnetic fluctuation observations of Van Allen Probe B during selected disturbed interval. (top) GSM and Minimum Variance (MV) coordinates filtered for frequencies between 0.1 and 1.0 Hz for a 10 s long interval starting at 04:44:55 (UT). (right) A hodogram for maximum (B_1) and intermediate (B_2) variance direction coordinates. The ratios of the eigenvalues of the minimum variance analysis are shown, as well as the resulting angle between the minimum variance direction and the local magnetic mean field. In the hodogram, blue and red squares represent the first and last points of the considered interval, respectively. (bottom) Same as Figure 6 (top) but for frequencies between 1 and 10 Hz during a shorter 1 s long interval starting at 04:44:58 (UT).

with respect to **k** [see, e.g., *Swanson*, 1989; *Stix*, 1992], the handedness of the waves in the hodograms does not indicate the polarization (right- or left-hand polarization) of the waves in the plasma frame. The plots shown in Figure 6 are representative of the whole data sets but do not exhibit the full range of fluctuation types within the data set. When considering more than 5 h of high-resolution magnetic field data with no clear frequency band for the fluctuations, it is possible to find a variety of results for the minimum variance analysis. In the case of turbulent broadband fluctuations spectra as shown in Figure 5 the use of hodograms it much less clear than when the observations exhibit clear bounded peaks in the frequency power spectrum. Thus, electromagnetic fluctuations observed during the storm are more consistent with a turbulent cascade interpretation than traveling coherent waves.

It is important to mention that some studies have found that in cometary environments [*Tsurutani et al.*, 1995, 1997] and other space plasmas observations [*Tsurutani et al.*, 2002, 2003] Alfvénic waves can phase steepen, creating both shorter and longer wavelength waves, dominating wave-wave interactions and then compromising the interpretation of the broadband fluctuations as the result of a turbulent cascade. Compared to our observations, in all the observations presented in *Tsurutani et al.* [1995, 1997] and *Tsurutani et al.* [2003] the magnetic fluctuations exhibit a clear bounded peak in the frequency power spectrum. In such cases the driver of the waves can be related to kinetic processes like ion-cyclotron resonant wave-particle interactions with local ion populations. Hence, the spectra can be interpreted as phase-steepening of EMIC waves as concluded by *Tsurutani et al.* [2003] and in one of the cases presented in *Tsurutani et al.* [1995, 1997]. In our case there is no evidence of a main driver of the broadband spectrum at any of the observed frequencies. Figure 5 exhibits no peaks within a more than 3 order range frequencies. In addition, in several of the selected intervals our observations show breaks in the spectral profiles (see Table 1). Thus, even though nonlinear effects such

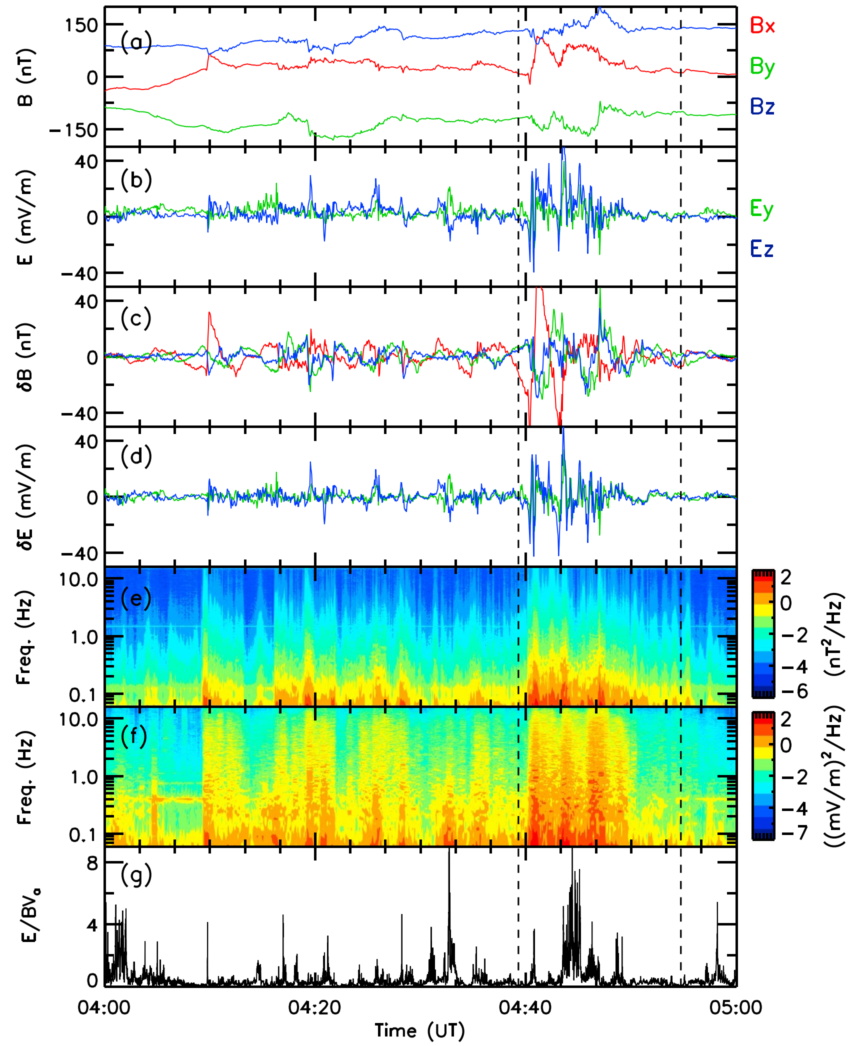

Figure 7. Van Allen Probe A (a) magnetic and (b) electric field components from 04:00 to 05:00 UT during the 14 November 2012 geomagnetic storm in mGSE coordinates. (c and d) Magnetic and electric fluctuations, respectively. Panels (e and f) Magnetic and electric fluctuations dynamic spectrograms, respectively. (g) Ratio between electric and magnetic field fluctuations. Red, green, and blue lines correspond to *x*, *y*, and *z* mGSE coordinates, respectively. Vertical lines marked disturbed interval studied in detail in section 2.2.

as phase steepening should be present, our interpretation of the observed broadband spectra as a turbulent cascade from large to small scales is consistent.

2.3. Electric Field Observations

To complement our analysis we consider electric field data obtained from the EFW instrument. During this particular storm both spacecraft experienced charging intervals in which the spacecraft potential decreased down to less than −100 V, degrading the quality of the electric field data. Thus, from the complete time interval considered (14 November 2012 between 01:30 to 06:00 UT) here we analyze the electric field observations from Van Allen Probe A between 04:00 and 05:00 UT.

Figures 7a and 7b shows magnetic field time series (at 32 vectors per second time resolution) from probe A between 04:00 and 05:00 UT expressed in modified geocentric solar ecliptic coordinates (mGSE), in which the X axis corresponds to the spacecraft spin axis $\hat{s}$ and the Y and Z axes lie in the spacecraft spin plane (in GSE $\hat{s} \sim (0.93786, -0.13898, 0.31795)$ during this time interval). The E_y and E_z components of the electric field are highly accurate in the spin plane. Figure 7a shows the three mGSE components of the magnetic field, corresponding to the proper rotation of **B** from GSM coordinates in Figure 3 to mGSE. We observe that the main effect is the shift of the B_x component from negative values in GSM to positive values in the mGSE frame.

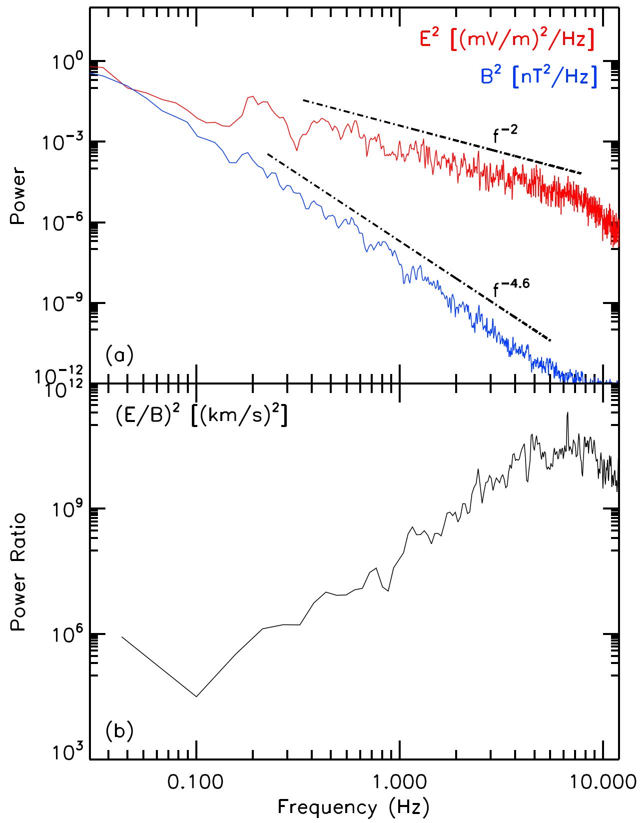

Figure 8. (a) Electric and magnetic power spectra and (b) electric to magnetic power ratio as function of frequency from disturbed interval between 04:40 and 04:55 UT.

Figure 7b shows the E_y and E_z mGSE components of the electric field with the spacecraft motion electric field $\mathbf{V}_{sc} \times \mathbf{B}$ removed. The electric field magnitude varies from a few mV/m to more than 40 mV/m, particularly during the disturbed interval between 04:40 and 04:55 UT bounded by vertical lines in the figure.

Following the same procedure as in section 2.1 we filter frequencies below 2 mHz and obtain the electric and magnetic fluctuations shown in Figures 7c and 7d. The electric field fluctuations exhibit patterns similar to the magnetic fluctuations. Therefore, the observed fluctuations are clearly electromagnetic and appear wherever the intermittent sudden changes of the magnetic field occur. Using an FFT algorithm, we compute the magnetic and electric dynamic spectrograms for overlapping intersecting intervals with 1024 points (32 s long), in the spacecraft frame as shown in Figures 7e and 7f. From the spectrograms we note that electric and magnetic field activities occur at the same time but that the power of the electric field fluctuations tends to be larger than that of the magnetic field and extends toward higher frequencies. As mentioned in section 1, one of the most important characteristics of the KAW mode is the large fluctuating electric field. In the absence of a unique and unambiguous measurement of the **k** vector when using single spacecraft time series (and in the lack of particle measurements to estimate the macroscopic plasma parameters still being carried out for the Van Allen Probes), probably the most important experimental quantity to differentiate between EMIC and KAW modes is the $\delta E/\delta B$ ratio [*Wygant et al.*, 2002; *Chaston et al.*, 2014]. In our study we have an estimation of the total density from the wave receivers of the EMFISIS Waves instrument (see Figure 3g), thus we can determine the local Alfvén speed based on the proton mass and the total density, namely, $V_A = B_0/\sqrt{4\pi n m_p}$. For the density range between $n = 10$ cm^{-3} and $n = 1$ cm^{-3} and a magnetic field magnitude $B_0 \sim$150 nT, the Alfvén speed varies between $V_A \sim$1035 km/s and $V_A \sim$3273 km/s. Figure 7g shows the $\delta E/(\delta B\, V_A)$ ratio as a function of time (where δE, δB correspond to the absolute value of the fluctuations amplitudes). From the figure it is clear that $\delta E/\delta B$ is larger than the local Alfvén speed during active intervals, as expected for KAWs [*Wygant et al.*, 2002; *Chaston et al.*, 2014]. The ratio is particularly enhanced during the disturbed interval between 04:40 and 04:55 UT, with the ratio of electric to magnetic perturbations 7 times greater than the Alfvén speed.

We now focus on the disturbed interval between 04:40 and 04:55 UT studied in section 2.2 and compare the spectral profiles of the electric and magnetic spectra in the frequency domain as shown in Figure 8. From the figure we confirm the conclusions made from the dynamic spectrograms in Figure 7. In addition, like the magnetic field, electric field fluctuations exhibit a power law spectral profile $\sim f^{-2}$. The ratio between electric and magnetic field fluctuations $\delta E/\delta B$ is an important signature to distinguish between ion-cyclotron waves and KAW. The former mode exhibit $\delta E/\delta B$ of the order of the local Alfvén speed, and in the case of the later $\delta E/\delta B$ is usually larger than the local Alfvén speed and increases with increasing frequency [*Chaston et al.*, 2014] or $k_\perp \rho_i$ value [*Voitenko and Goossens*, 2006]. In our results, in frequency domain (in the spacecraft frame) we observe that the electric power is much larger than the magnetic power for all frequencies above 0.1 Hz, and the ratio increases with increasing frequency until ~8 Hz, as expected for Doppler-shifted KAWs

[*Salem et al.*, 2012; *Chaston et al.*, 2014]. All these characteristics (in configuration space and Fourier domain) are consistent with the expected characteristic of KAW [*Hasegawa and Mima*, 1978; *Hollweg*, 1999; *Wygant et al.*, 2002; *Voitenko and Goossens*, 2006; *Salem et al.*, 2012; *Chaston et al.*, 2014]. In summary, our analysis accounts for electromagnetic fluctuations propagating highly oblique to the mean magnetic field, with large fluctuating electric field and magnetic compressibility and power law spectra that are steep power laws (in the spacecraft frame) indicating fluctuations in the dissipation range at kinetic scales. Thus, our results suggest the presence of Alfvénic turbulence in the dissipation range, in particular, kinetic Alfvén waves turbulence [*Hasegawa and Mima*, 1978; *Voitenko*, 1998a, 1998b; *Hollweg*, 1999].

3. Linear Plasma Waves Analysis

Even though our results suggest the presence of KAW turbulence during the main phase of the storm, the description of a particular spectrum as turbulent implies nonlinear wave-wave (such as parametric decays [*Voitenko*, 1998a] or three wave coupling [*Voitenko*, 1998b]) and wave-particle interactions resulting in a particular power law $f^{-\alpha}$ magnetic power spectrum. In the case of weakly dispersive KAW turbulence the steep spectral profile ($\alpha \sim 4$) may occur at spatial and temporal scales where the MHD turbulent cascade reaches ionic kinetic scales, wave-particle interactions dominate, and the magnetic energy is rapidly dissipated. This regime continues toward smaller subkinetic scales until another spectral break occurs, dividing weak and strong KAW turbulence where wave-wave interactions dominate and the spectral profile flattens [*Voitenko and De Keyser*, 2011].

The spectral profiles of the different turbulent regimes and the particular frequencies or wave numbers in which the spectral breaks occur, depend on the composition and properties of the plasma and the nature and level (nonlinearity) of the electromagnetic fluctuations and how the energy is dissipated [*Voitenko and De Keyser*, 2011]. Although our results suggest the presence of KAW in the weakly dispersive turbulent regime, they are still not conclusive. As mentioned in section 2.2, even though there is a wide variety of observations indicating that turbulence is ubiquitous in magnetized plasmas, it is very difficult to prove the presence of turbulence with single spacecraft measurements. However, recent experimental [*Howes et al.*, 2012] and Van Allen Probes observations [*Agapitov et al.*, 2015] provide evidence for nonlinear three-wave interaction between Alfvén in laboratory plasmas and between whistler and electron-acoustic waves in the outer radiation belt, respectively, establishing a robust basis for the use of the turbulence theoretical ideas in space plasma physics.

Turbulence theory is mainly written in terms of the interaction between waves with different wave numbers and different spatial scales. In contrast, all our analyses have been performed in the time and frequency domains, and our electric and magnetic spectral profiles are not expressed as functions of wave number. Obtaining such wave-number-dependent spectra implies knowing the particular dispersion relation of the observed fluctuations. The reduced nature of observations made by single spacecraft (meaning that the plasma sampling is restricted to one-dimensional time series from which spatial and temporal changes cannot be easily separated) makes determining an accurate wave vector $\mathbf{k}$ (including its magnitude) difficult. Thus, the identification of a particular dispersion relation $\omega(\mathbf{k})$ and the subsequent characterization of the particular wave modes also becomes difficult. An alternative approach is to compare the spectra as a function of frequency in the spacecraft frame with the theoretical spectra for the corresponding conditions. It is important to mention that, as usual in plasma wave studies, the results are given in the plasma frame and not in a moving frame like the spacecraft frame. A Doppler shift to transform the theoretical results to the frame in which observations were made is needed. The comparison between single-spacecraft observations (in which the Fourier spectra are obtained in the frequency domain) and theoretical calculations (in which frequency and wave vector spectra are available) is always difficult because the determination of the three components of the wave vector and the subsequent determination of turbulence is only possible when using at least four spacecraft in a noncoplanar configuration such as in studies made with Cluster mission observations [*Nykyri et al.*, 2004; *Sundkvist et al.*, 2005]. In the absence of an unambiguous determination of the wave vector, the calculation of the Doppler shift is not possible without the use of assumptions. Therefore, a unique characterization of the observed wave modes is never 100% accurate. Even with those limitations, theoretical and observational tools allow us to describe the waves and make conclusions regarding their nature.

A precise set of criteria to distinguish between the wave modes can be found if the wave properties are calculated from the eigenmodes of linear Vlasov theory [*Gary*, 1986; *Viñas et al.*, 2000] in which all the wave characteristics are known functions of frequency and wave vector. Our model consists of a uniform plasma composed of electrons, protons, He^+ ions, and O^+ ions, which are the dominant ion species in the ring current during the main phase of storms [*Hamilton et al.*, 1988; *Daglis et al.*, 1999; *Kamide and Chian* , 2007]. The medium is assumed to be neutral ($n_e = n_p + n_\alpha + n_o$) and to have zero currents in the direction of the mean field, where n_e, n_p, n_α, and n_o are the number density of electrons, protons, He^+ ions, and O^+ ions, respectively. We consider each species to have a zeroth-order velocity distribution function in the form of a Maxwellian:

$$f_j(v) = \frac{1}{\pi^{3/2}\alpha_j^3} e^{-\frac{v^2}{\alpha_j^2}} , \tag{1}$$

where $\alpha_j^2 = 2k_BT_j/m_j$ is square of the thermal speed of the jth species. T_j and m_j are temperature and mass of each species, and k_B is the Boltzmann constant.

The linearized kinetic dispersion equation for electromagnetic waves in a uniform, finite temperature plasma immersed in a constant mean magnetic field is given by

$$\Lambda(\omega, k, \theta; \mathrm{pp})\mathbf{E_k} = 0 \tag{2}$$

where Λ is the dispersion tensor, $\mathbf{E_k}$ are the electric field eigenmodes (fluctuations) and $k = |\mathbf{k}|$. The relationship between the electric and magnetic fields is given by Maxwell's equations. In equation (2) "pp" indicates plasma parameters such as densities, bulk velocities, and thermal speeds of each species. The appendix of *Viñas et al.* [2000] explains the theoretical approach in detail. Here we only note that the procedure to calculate the linear eigenmodes is well established to solve for the linear eigenmodes and associated electromagnetic fluctuation properties such as helicity, compressibility, and polarization spectra [*Gary*, 1986, 1993; *Viñas et al.*, 2000].

The solutions of the dispersion relation change with temperatures, densities, and angle of propagation θ among other plasma parameters (equation (2)). In terms of dimensionless quantities, the different solutions of equation (2) depend on plasma $\beta_j = 8\pi n_j k_B T_j/B_0^2$, the ratio between the local Alfvén speed $V_A = B_0/\sqrt{4\pi n_e m_p}$ (where B_0 is the mean field and m_p is the proton mass) and the speed of light c ($c_A = V_A/c$), and the abundances of each species $\eta_j = n_j/n_e$ with respect to the electrons. To compute these quantities, we consider values from EMFISIS observations (electron density, mean field magnitude, and angle of propagation) and typical values for temperatures and abundances during storm times. From the observation we note that during the interval of interest, total electron densities vary between $n_e \sim 1$ and ~ 10 cm^{-3} and also that the mean field magnitude is between 100 and 200 nT (see Figure 3).

In the ring current region (L between ~ 2 and 9), typical temperatures are $T \sim 10$ keV [*Kamide and Chian*, 2007] and O^+ abundances depend on the strength of the storm, varying between $\eta_o \sim 0.2$ and ~ 0.8 [*Hamilton et al.*, 1988; *Daglis*, 1997; *Daglis et al.*, 1999]. For this particular event (a moderate storm) we choose abundances of $\eta_o = 0.3$, $\eta_\alpha = 0.05$, and $\eta_p = 0.65$, we fix $B_0 = 150$ nT and consider an isothermal approximation $T = 10$ keV for all species. Using those parameters, we vary the total density by choosing three different values $n_e = 1$ (Case 1, low density), $n_e = 5$ (Case 2, medium density), and $n_e = 10$ cm^{-3} (Case 3, high density), to solve the dispersion relation in each case. It is important to mention that we are assuming that all density belongs to hot ($T \sim 10$ keV) ring current ions. Depending on the L shell and the position of the plasmapause, this selection of the plasma parameters may not be correct but it is reasonable for storm times, particularly for the atypical dropouts observed during this event. Several studies have shown that during storm time the plasmasphere is eroded and plumes can be formed carrying the cold plasma toward the noon magnetopause region [see, e.g., *Foster et al.*, 2014]. In addition, several empirical models predict the position of the plasmapause as a decreasing L shell value as a function of increasing K_p index for different Local Time sectors. For this storm $K_p \sim 6$ and then the predicted plasmapause location would be $L \sim 3.3$ [see, e.g., *Moldwin et al.*, 2002]. Hence, as during the time interval of interest $L > 4$, our selection is reasonable. A summary of the chosen parameters is presented in Table 2. For these choices we observe that β values vary between 0.054 and 1.116 which is a sufficiently large range of possible parameters. Let us note that this range in β is also obtainable from different values of temperatures or abundances. If we fix T to 10 keV and vary n_e from 1 cm^{-3} to 10 cm^{-3}, we would obtain the same beta values as by fixing $n_e = 10$ cm^{-3} and changing T from 1 keV to 10 keV and then consequently obtain the same results from the kinetic theory analysis. Here we decided to vary only the quantities obtained using the in situ observation, which in this case is the total density. For all three cases we fix the propagation angle to

Table 2. Linear Theory Calculation Parameters[a]

Case	Total Density (cm^{-3})	$C_A = V_A/c$	Species	β
			H^+	0.116
Case 1	1	1.091×10^{-2}	He^+	0.009
			O^+	0.054
			H^+	0.582
Case 2	5	4.878×10^{-3}	He^+	0.045
			O^+	0.269
			H^+	1.116
Case 3	10	3.449×10^{-3}	He^+	0.090
			O^+	0.537

[a]In all cases $B_0 = 150$ nT, $T = 10$ keV, $\eta_{H^+} = 0.65$, $\eta_{He^+} = 0.05$, and $\eta_{O^+} = 0.3$.

$\theta = 60°$, which is the average propagation angle obtained from MVA (see Table 1). Using the parameters from Table 2, we solved the dispersion relation equation (2) and obtained the eigenfrequencies and corresponding eigenvectors for each mode. From all possible solutions we selected the O^+-Alfvén and the H^+-Alfvén modes and constructed the spectra of the magnetic compressibility C_k, polarization P_k, and magnetic helicity σ_k in the plasma frame.

Figure 9 shows frequency and magnetic properties spectra, all as a function of wave number for each ion Alfvén mode solution: Case 1 (left), Case 2 (middle) and Case 3 (right). From top to bottom the panels show the frequency, polarization (normalized to its maximum value), magnetic helicity, and magnetic compressibility. To test the presence of KAW turbulence in the weakly dispersive range $k_\perp \rho_i \lesssim 1$, we express all spectral quantities as functions of $k_\perp \rho_p$; namely, the perpendicular wave number $k_\perp = |\mathbf{k}|/\sin(\theta)$ normalized to the proton gyroradius $\rho_p = \alpha_p/\Omega_p$, where Ω_p is the proton gyrofrequency. In the absence of differential streaming between species the dispersion plots for the real part of the frequency show the frequency band associated with each ion independent of the value of the density. Also, as there is no free energy source the imaginary part of the frequencies corresponds only to damping. As density increases (from Case 1 to Case 3) the higher values of plasma density shift the three Alfvén branches to lower frequencies and higher damping rates.

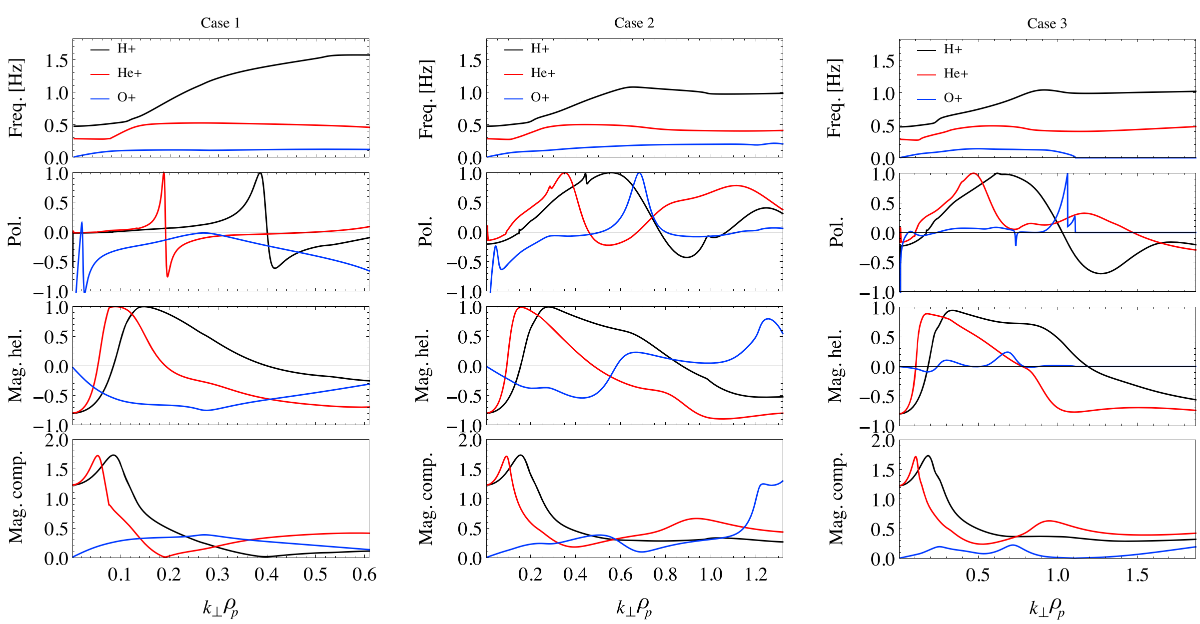

Figure 9. Theoretical calculations of complex frequency and spectral properties of Alfvénic wave modes as a function of perpendicular wave number for (left) low, (middle) medium, and (right) high total density. From top to bottom, panels show frequency, normalized polarization, magnetic helicity, and magnetic compressibility, respectively. Black, red, and blue lines represent H^+, He^+, and O^+ Alfvén modes solutions. Wave numbers are expressed in units of the proton gyroradius.

Whatever the case, the real frequencies are mainly below 1 Hz for $k_\perp \rho_p \lesssim 1$. An estimation of the Doppler shift (the $\mathbf{k} \cdot \mathbf{V_o}$ term) can be made using a few assumptions. If we consider that $\mathbf{V_o}$ is the $\mathbf{E} \times \mathbf{B}_0$ drift, using the observed values $E \lesssim 45$ mV/m and $B_0 \sim 150$ nT, then we obtain $V_0 \lesssim 300$ km/s. On the other hand, with the chosen parameters $\rho_p \sim 100$ km. Considering KAW with $k_\perp \rho_p \sim 1$, then $k_\perp \sim 10^{-2}$ km^{-1}. Thus, the Doppler shift $|\mathbf{k} \cdot \mathbf{V_o}| = k_\perp V_0$ will be of the order of a few Hz, which is consistent with the differences between the observed frequencies in the spacecraft frame (see, e.g., Figure 8) and the theoretical frequencies obtained from Vlasov linear theory (see Figure 9).

For the three Alfvén modes we search for the signature characteristics of KAW mode such as positive (right-handed) polarization and magnetic helicity and compare the theoretical results with the observations. From Figure 9 we notice that except for Case 1 all three modes have a wave number range in which both polarization and magnetic helicity are positive; i.e., the modes share the same properties of right-handed KAW. As density increases the range shifts toward higher $k_\perp$ (higher frequencies), but in all the cases the condition $k_\perp \rho_p \lesssim 1$ is fulfilled. Looking more in detail, we observe that for all of the three modes (black, red, and blue curves in Figure 9) the polarization and the magnetic helicity wave number spectrum change sign several times. However, except for case 1 for almost all $k_\perp$ values at least one of the three modes has positive polarization and positive magnetic helicity, both consistent with the properties of KAW modes. It is important to mention that the theoretical ideas about kinetic Alfvén waves have been obtained considering simple cases in which the plasma is composed only of electrons and protons. In the present case the presence of other ion species leads to a much more complex situation. The exact description of KAWs in multispecies plasmas is an interesting and challenging theoretical problem that goes beyond the scope of the present work. However, in our calculations the properties of the three modes are more consistent with KAWs than with EMIC, which is also consistent with the observations. Finally, the magnetic compressibility spectrum shows compressive modes with $0.5 < C_k < 1.5$ for H^+ and He^+ modes. Although they have been calculated in the plasma frame and not in each spacecraft frame. As mentioned before, the waves are not Doppler shifted much in frequency and, subsequently, the polarization in both reference frames should be the same. All these features show the presence of KAW from the theoretical point of view, are consistent with the observations, and therefore reinforce the interpretation of this event as weak KAW turbulence. In addition, even though the analysis presented here is based on a simple approximation of the local plasma conditions, the approximations are good enough to answer the question about whether the conditions allow the presence of the KAW mode or not.

4. Discussion and Conclusions

We used EMFISIS and EFW Van Allen Probes data sets to study electric and magnetic field fluctuations during the main phase of the 14 November 2012 geomagnetic storm, approximately between 01:30 and 06:00 UT. We observed intermittency between intervals with small magnetic field amplitudes and dominant B_x GSM component and short disturbed intervals of about 15 min long, with large GSM B_y and B_z components and weak B_x, and fluctuations with amplitudes larger than 15 nT (see Figure 3). Consistently, power spectrograms (see Figure 4) show more magnetic activity during disturbed intervals, corresponding to a broadband spectrum with most of the power for frequencies below H^+, He^+, and O^+ local gyrofrequencies in the spacecraft frame. We found that most of the time fluctuations are highly oblique, propagating at about 60°with respect to the mean field direction (with an ambiguity in the sign), and the compressibility is of order 1 (see Figure 4). In addition, observations indicate that electric field fluctuations are present wherever the magnetic field is disturbed and large electric field fluctuations follow the same pattern of quiet and disturbed intervals we defined for the magnetic field (see Figure 7) and that the ratio between electric and magnetic fluctuation amplitudes can be several times the local Alfvén speed. All these results suggest the presence of a broadband spectrum of kinetic Alfvén waves during the main phase of the storm.

From the whole magnetic field time series we selected five short intervals (three disturbed and two quiet) of 10 to 15 min long to study the propagation and spectral characteristics of the fluctuations during quiet and disturbed intervals, and their differences and similarities (see Table 1). For all intervals and both spacecraft the minimum variance and compressibility are similar, but the compressibility standard deviation is much higher for disturbed periods, which could mean the presence of more field-aligned perturbations. Furthermore, during quiet intervals the total power of the fluctuations is less than 0.1 nT^2 (3 orders of magnitude less than in disturbed intervals), which is consistent with our description of disturbed and quiet intervals based only on the properties of the magnetic field in real space. In addition, at frequencies below 2 Hz, frequency power spectra (see Figure 5) correspond to power law frequency spectrum $f^{-\alpha}$, with $4 < \alpha < 5$, power laws steeper than the Kolmogorov $f^{-5/3}$, indicating fluctuations in the dissipation range and wave-particle interactions [see, e.g., *Bruno and Carbone*, 2013, and references therein]. For higher frequencies the spectral profile flattens and $1.1 < \alpha < 1.7$. For both spacecraft the frequency power laws are consistent with KAW turbulence in the weakly dispersive range or weak kinetic Alfvén wave turbulence [*Voitenko*, 1998a, 1998b; *Voitenko and De Keyser*, 2011], corresponding to the intermediate frequency range above the inertial range, and below the fully developed KAW turbulence at subkinetic scales ($k_\perp \rho_i > 1$). Consistently with the properties of KAW modes, the electric power is larger than the magnetic power for all frequencies above 0.1 Hz, and the ratio increases with increasing frequency (see Figure 8). While the ellipticity and angle of polarization spectra from both quiet and disturbed intervals are consistent with this interpretation, magnetic helicity and degree of polarization spectra from both, quiet and disturbed subintervals are not sufficiently clear to be conclusive. To further characterize the fluctuations, we compute hodograms to study the waveforms and the minimum variance direction for a few seconds within the selected disturbed intervals. From the hodograms we observe that for frequencies 0.1 Hz $< f <$ 1.0 Hz the waves seem to exhibit an elliptical polarization in the spacecraft frame (see Figure 6).

We also performed a Vlasov linear theory analysis based on observed total density (see Figure 3g) and typical ring current parameters during storm times. We computed the dispersion curves and spectral characteristics for low, medium, and high density cases (see Table 2). Except for the low density case, theoretical results are consistent with the presence of magnetic compressive kinetic Afvén waves with right-handed polarization and positive magnetic helicity (in the plasma frame) as shown in Figure 9. As the density increases the KAW modes shift toward higher $k_\perp$ (higher frequencies), but in all the cases the condition $k_\perp \rho_p \lesssim 1$ is fulfilled. All these features show the presence of KAW from the theoretical point of view, which is consistent with the observations and reinforces the interpretation of the electromagnetic fluctuations as weak KAW turbulence.

Turbulence theory provides a robust explanation concerning how the energy is transferred from large to small scales due to a cascade of nonlinear wave-wave interactions [*Bruno and Carbone*, 2013] and also wave-particle interactions at kinetic scales. In particular, recent studies of turbulence in laboratory plasmas [*Howes et al.*, 2012], and observations of three-waves interactions in the radiation belts [*Agapitov et al.*, 2015] provide evidence and a consistent framework for the application of these theoretical ideas in space and astrophysical plasmas. As discussed in section 2.2, even though turbulence is ubiquitous in laboratory [*Howes et al.*, 2012] space and astrophysical plasmas, such as the solar wind [*Leamon et al.*, 2000; *Bale et al.*, 2005; *Bruno and Carbone*, 2013] and the Earth's magnetosphere [*Nykyri et al.*, 2004; *Sundkvist et al.*, 2005; *Agapitov et al.*, 2015], other ideas exist and there are a number of observations that can also be explained as the result of other nonlinear effects (such as phase-steepening) besides turbulent cascades [*Tsurutani et al.*, 1995, 1997, 2002, 2003]. However, in our observations there is no evidence for a main driver of the broadband spectrum at any of the observed frequencies. The magnetic power frequency spectra exhibit no peaks within more than 3 orders of magnitude, and in more than half of the selected intervals the spectra present spectral breaks (see Table 1) suggesting a transition between steep dissipation due to wave-particle interactions and a flatter high-frequency regime in which wave-wave interactions should be dominant.

Weak KAW turbulence theory suggests that the steep spectral profile and the double spectral break (from inertial range to weakly dispersive and from weakly dispersive to strong KAW regime) are related to nonadiabatic ion heating and other nonlinear wave-particle interactions [*Voitenko and De Keyser*, 2011]. The observed large fluctuating electric field may also indicate energy dissipation due to Landau damping. The electrostatic component of the oblique fluctuations (particularly electric field fluctuations along the mean field) can affect the particles via Landau resonances, and thus, the fluctuations can be absorbed via Landau damping. This effect becomes larger as the wave normal angle increases. In fact, this effect is specially important for KAW modes, see, for example, *Hollweg* [1999], and it is considered as one of the ways in which energy can flow from ion to electron scales. Correlations between electromagnetic and particle velocity fluctuations, such as cross-helicity spectrum [*Matthaeus and Goldstein*, 1982; *Viñas et al.*, 1984], are necessary to further characterize the type of the waves and excited modes. We expect to increase the scope of the current work using plasma data (such as abundances and particle moments) not yet available for this event. A more complete analysis will help us to understand more details of the wave-particle interactions, the energy source of the observed fluctuations, and the role of turbulence during geomagnetic storms.

Acknowledgments
We acknowledge Craig Kletzing for useful discussions and for providing data from the EMFISIS instrument suite of the Van Allen Probes Mission. Data sets were provided by the Space Physics Data Facility at Goddard Space Flight Center through their Coordinated Data Analysis Web (http://cdaweb.gsfc.nasa.gov). We would like to thank Kyoung-Joo Hwang, Alex Glocer, Elizabeth MacDonald, and Bea Gallardo-Lacourt for useful discussions. Portions of this work were performed under the support of JHU/APL contract 921647 under NASA Prime contract NAS5-01072. A portion of this work was supported by Van Allen Probe mission funds at NASA/GSFC. We also thank Comisión Nacional de Ciencia y Tecnología (CONICyT, Chile) for providing financial support for postdoctoral (P.S.M.) and doctoral (V.A.P.) fellows.

M. Balikhin thanks Anton Artemyev and two anonymous reviewers for their assistance in evaluating this paper.

References

Agapitov, O. V., V. Krasnoselskikh, F. S. Mozer, A. V. Artemyev, and A. S. Volokitin (2015), Generation of nonlinear electric field bursts in the outer radiation belt through the parametric decay of whistler waves, *Geophys. Res. Lett.*, *42*, 3715–3722, doi:10.1002/2015GL064145.

Anderson, B. J., R. E. Erlandson, and L. J. Zanetti (1992a), A statistical study of Pc 1–2 magnetic pulsations in the equatorial magnetosphere: 1. Equatorial occurrence distributions, *J. Geophys. Res.*, *97*(A3), 3075–3088, doi:10.1029/91JA02706.

Anderson, B. J., R. E. Erlandson, and L. J. Zanetti (1992b), A statistical study of Pc 1–2 magnetic pulsations in the equatorial magnetosphere: 2. Wave properties, *J. Geophys. Res.*, *97*(A3), 3089–3101, doi:10.1029/91JA02697.

Anderson, B. J., R. E. Denton, and S. A. Fuselier (1996), On determining polarization characteristics of ion cyclotron wave magnetic field fluctuations, *J. Geophys. Res.*, *101*(A6), 13,195–13,213, doi:10.1029/96JA00633.

Bale, S. D., P. J. Kellogg, F. S. Mozer, T. S. Horbury, and H. Reme (2005), Measurement of the electric fluctuation spectrum of magnetohydrodynamic turbulence, *Phys. Rev. Lett.*, *94*, 215,002, doi:10.1103/PhysRevLett.94.215002.

Bräysy, T., K. Mursula, and G. Marklund (1998), Ion cyclotron waves during a great magnetic storm observed by Freja double-probe electric field instrument, *J. Geophys. Res.*, *103*(A3), 4145–4155, doi:10.1029/97JA02820.

Bruno, R., and V. Carbone (2013), The solar wind as a turbulence laboratory, *Living Rev. Sol. Phys.*, *10*, 2, doi:10.12942/lrsp-2013-2.

Chaston, C. C., T. D. Phan, J. W. Bonnell, F. S. Mozer, M. Acuña, M. L. Goldstein, A. Balogh, M. Andre, H. Reme, and A. Fazakerley (2005), Drift-kinetic Alfvén waves observed near a reconnection X line in the Earth's magnetopause, *Phys. Rev. Lett.*, *95*, 65,002, doi:10.1103/PhysRevLett.95.065002.

Chaston, C. C., V. Genot, J. W. Bonnell, C. W. Carlson, J. P. McFadden, R. E. Ergun, R. J. Strangeway, E. J. Lund, and K. J. Hwang (2006), Ionospheric erosion by Alfvén waves, *J. Geophys. Res.*, *111*, A03206, doi:10.1029/2005JA011367.

Chaston, C. C., J. W. Bonnell, L. Clausen, and V. Angelopoulos (2012), Correction to "Energy transport by kinetic-scale electromagnetic waves in fast plasma sheet flows", *J. Geophys. Res.*, *117*, A12205, doi:10.1029/2012JA018476.

Chaston, C. C., et al. (2014), Observations of kinetic scale field line resonances, *Geophys. Res. Lett.*, *41*, 209–215, doi:10.1002/2013GL058507.

Cornwall, J. M. (1965), Cyclotron instabilities and electromagnetic emission in the ultra low frequency and very low frequency ranges, *J. Geophys. Res.*, *70*(1), 61–69, doi:10.1029/JZ070i001p00061.

Daglis, I. A. (1997), The role of magnetosphere-ionosphere coupling in magnetic storm dynamics, in *Magnetic Storms*, pp. 107–116, AGU, Washington, D. C., doi:10.1029/GM098p0107.

Daglis, I. A., R. M. Thorne, W. Baumjohann, and S. Orsini (1999), The terrestrial ring current: Origin, formation and decay, *Rev. Geophys.*, *37*(4), 407–438, doi:10.1029/1999RG900009.

Denton, R. E., B. J. Anderson, G. Ho, and D. C. Hamilton (1996), Effects of wave superposition on the polarization of electromagnetic ion cyclotron waves, *J. Geophys. Res.*, *101*(A11), 24,869–24,885, doi:10.1029/96JA02251.

Erlandson, R. E., and A. J. Ukhorskiy (2001), Observations of electromagnetic ion cyclotron waves during geomagnetic storms: Wave occurrence and pitch angle scattering, *J. Geophys. Res.*, *106*(A3), 3883–3895, doi:10.1029/2000JA000083.

Erlandson, R. E., L. J. Zanetti, T. A. Potemra, L. P. Block, and G. Holmgren (1990), Viking magnetic and electric field observations of Pc 1 waves at high latitudes, *J. Geophys. Res.*, *95*(A5), 5941–5955, doi:10.1029/JA095iA05p05941.

Foster, J. C., P. J. Erickson, A. J. Coster, S. Thaller, J. Tao, J. R. Wygant, and J. W. Bonnell (2014), Storm time observations of plasmasphere erosion flux in the magnetosphere and ionosphere, *Geophys. Res. Lett.*, *41*, 762–768, doi:10.1002/2013GL059124.

Fowler, R. A., B. J. Kotick, and R. D. Elliott (1967), Polarization analysis of natural and artificially induced geomagnetic micropulsations, *J. Geophys. Res.*, *72*(11), 2871–2883, doi:10.1029/JZ072i011p02871.

Gamayunov, K. V., G. V. Khazanov, M. W. Liemohn, M.-C. Fok, and A. J. Ridley (2009), Self-consistent model of magnetospheric electric field, ring current, plasmasphere, and electromagnetic ion cyclotron waves: Initial results, *J. Geophys. Res.*, *114*, A03221, doi:10.1029/2008JA013597.

Gary, S. P. (1986), Low frequency waves in a high-beta collisionless plasma: Polarization, compressibility and helicity, *J. Plasma Phys.*, *35*(A4), 431–447, doi:10.1029/93JA02867.

Gary, S. P. (1992), The mirror and ion cyclotron anisotropy instabilities, *J. Geophys. Res.*, *97*(A6), 8519–8529, doi:10.1029/92JA00299.

Gary, S. P. (1993), Cambridge Univ. Press.

Glocer, A., N. Buzulukova, M. H. Fok, D. G. Sibeck, and S. Chen (2013), Multi-physics simulations of Van Allen Probes observations of November 14th 2012, Abstract SM33C-05 presented at 2013 Fall Meeting, AGU, San Francisco, Calif., 9–13 Dec.

Gomberoff, L., and R. Elgueta (1991), Resonant acceleration of α-particles by ion-cyclotron waves in the solar wind, *J. Geophys. Res.*, *96*, 9801–9804, doi:10.1029/91JA00613.

Gomberoff, L., and J. A. Valdivia (2003), Ion cyclotron instability due to the thermal anisotropy of drifting ion species, *J. Geophys. Res.*, *108*(A1), 1050, doi:10.1029/2002JA009576.

Gonzalez, W. D., J. A. Joselyn, Y. Kamide, H. W. Kroehl, G. Rostoker, B. T. Tsurutani, and V. M. Vasyliunas (1994), What is a geomagnetic storm?, *J. Geophys. Res.*, *99*(A4), 5771–5792, doi:10.1029/93JA02867.

Hamilton, D. C., G. Gloeckler, F. M. Ipavich, W. Stüdemann, B. Wilken, and G. Kremser (1988), Ring current development during the great geomagnetic storm of February 1986, *J. Geophys. Res.*, *93*(A12), 14,343–14,355, doi:10.1029/JA093iA12p14343.

Hasegawa, A. (1976), Particle acceleration by MHD surface wave and formation of aurora, *J. Geophys. Res.*, *81*(28), 5083–5090, doi:10.1029/JA081i028p05083.

Hasegawa, A., and K. Mima (1978), Anomalous transport produced by kinetic Alfvén wave turbulence, *J. Geophys. Res.*, *83*(A3), 1117–1123, doi:10.1029/JA083iA03p01117.

Hollweg, J. V. (1999), Kinetic Alfvén wave revisited, *J. Geophys. Res.*, *A7*, 14,811–14,819, doi:10.1029/1998JA900132.

Howes, G. G., D. J. Drake, K. D. Nielson, T. A. Carter, C. A. Kletzing, and F. Skiff (2012), Toward astrophysical turbulence in the laboratory, *Phys. Rev. Lett.*, *109*, 255,001, doi:10.1103/PhysRevLett.109.255001.

Huang, G.-L., D.-Y. Wang, D.-J. Wu, H. de Féraudy, D. Le Quéau, M. Volwerk, and B. Holback (1997), The eigenmode of solitary kinetic Alfvén waves observed by Freja satellite, *J. Geophys. Res.*, *102*(A4), 7217–7224, doi:10.1029/96JA02607.

Hwang, K.-J., et al. (2015), The global context of the 14 November 2012 storm event, *J. Geophys. Res.*, *120*, 1939–1956, doi:10.1002/2014JA020826.

Iyemori, T., and K. Hayashi (1989), Pc 1 micropulsations observed by Magsat in the ionospheric F region, *J. Geophys. Res.*, *94*(A1), 93–100, doi:10.1029/JA094iA01p00093.

Johnson, J. R., and C. Z. Cheng (2001), Stochastic ion heating at the magnetopause due to kinetic Alfvén waves, *Geophys. Res. Lett.*, *28*(23), 4421–4424, doi:10.1029/2001GL013509.

Johnson, J. R., C. Z. Cheng, and P. Song (2001), Signatures of mode conversion and kinetic Alfvén waves at the magnetopause, *Geophys. Res. Lett.*, *28*(2), 227–230, doi:10.1029/2000GL012048.

Kamide, Y., and A. C. L. Chian (Eds.) (2007), *Handbook of the solar-terrestrial environment*, Springer, Berlin, doi:10.1007/978-3-540-46315-3.

Keika, K., K. Takahashi, A. Y. Ukhorskiy, and Y. Miyoshi (2013a), Global characteristics of electromagnetic ion cyclotron waves: Occurrence rate and its storm dependence, *J. Geophys. Res. Space Physics*, *118*, 4135–4150, doi:10.1002/jgra.50385.

Keika, K., L. M. Kistler, and P. C. Brandt (2013b), Energization of O^+ ions in the Earth's inner magnetosphere and the effects on ring current buildup: A review of previous observations and possible mechanisms, *J. Geophys. Res. Space Physics*, *118*, 4441–4464, doi:10.1002/jgra.50371.

Kennel, C. F., and H. E. Petschek (1966), Limit on stably trapped particle fluxes, *J. Geophys. Res.*, *71*, 1–28, doi:10.1029/JZ071i001p00001.

Khazanov, G. V. (2011), *Kinetic Theory of the Inner Magnetospheric Plasma*, Springer, New York, doi:10.1007/978-1-4419-6797-8.

Khazanov, G. V., K. V. Gamayunov, D. L. Gallagher, J. U. Kozyra, and M. W. Liemohn (2007), Self-consistent model of magnetospheric ring current and propagating electromagnetic ion cyclotron waves: 2. Wave-induced ring current precipitation and thermal electron heating, *J. Geophys. Res.*, *112*, A04209, doi:10.1029/2006JA012033.

Kletzing, C., et al. (2013), The electric and magnetic field instrument suite and integrated science (EMFISIS) on RBSP, *Space Sci. Rev.*, *179*, 127–181, doi:10.1007/s11214-013-9993-6.

Kloecker, N., H. Luehr, A. Korth, and P. Robert (1985), Observation of kinetic Alfvén waves excited at substorm onset, *J. Geophys.*, *57*, 65–71.

Kurth, W. S., S. De Pascuale, J. B. Faden, C. A. Kletzing, G. B. Hospodarsky, S. Thaller, and J. R. Wygant (2015), Electron densities inferred from plasma wave spectra obtained by the Waves instrument on Van Allen Probes, *J. Geophys.*, *120*, 904–914, doi:10.1002/2014JA020857.

LaBelle, J., R. A. Treumann, W. Baumjohann, G. Haerendel, N. Sckopke, G. Paschmann, and H. Lühr (1988), The duskside plasmapause/ring current interface: Convection and plasma wave observations, *J. Geophys. Res.*, *93*(A4), 2573–2590, doi:10.1029/JA093iA04p02573.

Leamon, R. J., W. H. Matthaeus, C. W. Smith, G. P. Zank, D. J. Mullan, and S. Oughton (2000), MHD-driven kinetic dissipation in the solar wind and corona, *Astrophys. J.*, *537*(2), 1054, doi:10.1086/309059.

Lee, J. H., L. Chen, V. Angelopoulos, and R. M. Thorne (2012), THEMIS observations and modeling of multiple ion species and EMIC waves: Implications for a vanishing He^+ stop band, *J. Geophys. Res.*, *117*, A06204, doi:10.1029/2012JA017539.

Lee, L. C., J. R. Johnson, and Z. W. Ma (1994), Kinetic Alfvén waves as a source of plasma transport at the dayside magnetopause, *J. Geophys. Res.*, *99*(A9), 17,405–17,411, doi:10.1029/94JA01095.

Lysak, R. L. (2008), On the dispersion relation for the kinetic Alfvén wave in an inhomogeneous plasma, *Phys. Plasmas*, *15*, 62,901, doi:10.1063/1.2918742.

Matthaeus, W. H., and M. L. Goldstein (1982), Measurement of the rugged invariants of magnetohydrodynamic turbulence in the solar wind, *J. Geophys. Res.*, *87*(A8), 6011–6028, doi:10.1029/JA087iA08p06011.

Mauk, B., N. Fox, S. Kanekal, R. Kessel, D. Sibeck, and A. Ukhorskiy (2012), Science objectives and rationale for the radiation belt storm probes mission, *Space Sci. Rev.*, *179*, 3–27, doi:10.1007/s11214-012-9908-y.

Mauk, B. H. (1982), Helium resonance and dispersion effects on geostationary Alfvén/Ion cyclotron waves, *J. Geophys. Res.*, *87*(A11), 9107–9119, doi:10.1029/JA087iA11p09107.

Means, J. D. (1972), Use of the three-dimensional covariance matrix in analyzing the polarization properties of plane waves, *J. Geophys. Res.*, *77*(28), 5551–5559, doi:10.1029/JA077i028p05551.

Min, K., J. Lee, K. Keika, and W. Li (2012), Global distribution of EMIC waves derived from THEMIS observations, *J. Geophys. Res.*, *117*, A05219, doi:10.1029/2012JA017515.

Moldwin, M. B., L. Downward, H. K. Rassoul, R. Amin, and R. R. Anderson (2002), A new model of the location of the plasmapause: CRRES results, *J. Geophys. Res.*, *107*(A11), 1339, doi:10.1029/2001JA009211.

Mourenas, D., A. V. Artemyev, O. V. Agapitov, and V. Krasnoselskikh (2013), Analytical estimates of electron quasi-linear diffusion by fast magnetosonic waves, *J. Geophys. Res.*, *118*, 3096–3112, doi:10.1002/jgra.50349.

Mursula, K., J. Kangas, and T. Pikkarainen (1994), Properties of structured and unstructured Pc1 pulsations at high latitudes: variation over the 21st solar cycle, in *Solar Wind Sources of Magnetospheric Ultra-Low-Frequency Waves*, pp. 409–415, AGU, Washington, D. C., doi:10.1029/GM081p0409.

Nykyri, K., et al. (2004), Cluster observations of magnetic field fluctuations in the high-altitude cusp, *Ann. Geophys.*, *22*(7), 2413–2429, doi:10.5194/angeo-22-2413-2004.

Omura, Y., and Q. Zhao (2013), Relativistic electron microbursts due to nonlinear pitch angle scattering by EMIC triggered emissions, *J. Geophys. Res. Space Physics*, *118*, 5008–5020, doi:10.1002/jgra.50477.

Perraut, S., O. Le Contel, A. Roux, R. Pellat, A. Korth, Ø. Holter, and A. Pedersen (2000), Disruption of parallel current at substorm breakup, *Geophys. Res. Lett.*, *27*(24), 4041–4044, doi:10.1029/2000GL000054.

Rankin, D., and R. Kurtz (1970), Statistical study of micropulsation polarizations, *J. Geophys. Res.*, *75*(28), 5444–5458, doi:10.1029/JA075i028p05444.

Salem, C. S., G. G. Howes, D. Sundkvist, S. D. Bale, C. C. Chaston, C. H. K. Chen, and F. S. Mozer (2012), Identification of kinetic Alfvén wave turbulence in the solar wind, *Astrophys. J. Lett.*, *745*, L9, doi:10.1088/2041-8205/745/1/L9.

Santolík, O., J. S. Pickett, D. A. Gurnett, M. Maksimovic, and N. Cornilleau-Wehrlin (2002), Spatiotemporal variability and propagation of equatorial noise observed by Cluster, *J. Geophys. Res.*, *107*(A12), 1495, doi:10.1029/2001JA009159.

Sonnerup, B. U. Ö., and L. J. Cahill (1967), Magnetopause structure and attitude from Explorer 12 observations, *J. Geophys. Res.*, *72*(1), 171–183, doi:10.1029/JZ072i001p00171.

Sonnerup, B. U. Ö., and M. Scheible, (1998), Analysis methods for multi-spacecraft data, ESA ISSI Sci. Rep., SR-001, vol. 1, chap. 8, Minimum and Maximum Variance Analysis, pp. 185–220, ESA Publications Division, Noordwidjk, Netherlands.

Stix, T. (1992), *Waves in Plasmas*, Am. Inst. of Phys., New York.

Stratton, J., R. Harvey, and G. Heyler (2013), Mission overview for the radiation belt storm probes mission, *Space Sci. Rev.*, *179*, 29–57, doi:10.1007/s11214-012-9933-x.

Stringer, T. E. (1963), Low frequency waves in an unbounded plasma, *J. Nucl. Energy, Part C Plasma Phys.*, *5*, 89–107, doi:10.1088/0368-3281/5/2/304.

Summers, D., and R. M. Thorne (2003), Relativistic electron pitch-angle scattering by electromagnetic ion cyclotron waves during geomagnetic storms, *J. Geophys. Res.*, *108*(A4), 1143, doi:10.1029/2002JA009489.

Sundkvist, D., V. Krasnoselskikh, P. K. Shukla, A. Vaivads, M. Andre, S. Buchert, and H. Reme (2005), In situ multi-satellite detection of coherent vortices as a manifestation of Alfvenic turbulence, *Nature*, *436*(7052), 825–828, doi:10.1038/nature03931.

Swanson, D. (1989), *Plasmas Waves*, Acad. Press, San Diego, Calif.

Thorne, R. M., and R. B. Horne (1992), The contribution of ion-cyclotron waves to electron heating and SAR-arc excitation near the storm-time plasmapause, *Geophys. Res. Lett.*, *19*(4), 417–420, doi:10.1029/92GL00089.

Thorne, R. M., and R. B. Horne (1994), Energy transfer between energetic ring current H^+ and O^+ by electromagnetic ion cyclotron waves, *J. Geophys. Res.*, *99*(A9), 17,275–17,282, doi:10.1029/94JA01007.

Thorne, R. M., and R. B. Horne (1997), Modulation of electromagnetic ion cyclotron instability due to interaction with ring current O^+ during magnetic storms, *J. Geophys. Res.*, *102*(A7), 14,155–14,163, doi:10.1029/96JA04019.

Thorne, R. M., and C. F. Kennel (1971), Relativistic electron precipitation during magnetic storm main phase, *J. Geophys. Res.*, *76*, 4446–4453, doi:10.1029/JA076i019p04446.

Tsurutani, B. T., K. H. Glassmeier, and F. M. Neubauer (1995), An intercomparison of plasma turbulence at three comets: Grigg-Skjellerup, Giacobini-Zinner, and Halley, *Geophys. Res. Lett.*, *22*(9), 1149–1152, doi:10.1029/95GL00806.

Tsurutani, B. T., K. H. Glassmeier, and F. M. Neubauer (1997), A review of nonlinear Low Frequency (LF) wave observations in space plasmas: On the development of plasma turbulence, in *Nonlinear Waves and Chaos in Space Plasmas*, vol. 29, chap. 1., pp. 1–44, Terra Sci. Publ. Comp., Tokyo, Jpn.

Tsurutani, B. T., C. Galvan, J. K. Arballo, D. Winterhalter, R. Sakurai, E. J. Smith, B. Buti, G. S. Lakhina, and A. Balogh (2002), Relationship between discontinuities, magnetic holes, magnetic decreases, and nonlinear Alfvén waves: Ulysses observations over the solar poles, *Geophys. Res. Lett.*, *29*(11), 1528, doi:10.1029/2001GL013623.

Tsurutani, B. T., B. Dasgupta, J. K. Arballo, G. S. Lakhina, and J. S. Pickett (2003), Magnetic field turbulence, electron heating, magnetic holes, proton cyclotron waves, and the onsets of bipolar pulse (electron hole) events: A possible unifying scenario, *Nonlinear Proc. Geophys.*, *10*(1/2), 27–35, doi:10.5194/npg-10-27-2003.

Viñas, A. F., M. L. Goldstein, and M. H. Acuña (1984), Spectral analysis of magnetohydrodynamic fluctuations near interplanetary shocks, *J. Geophys. Res.*, *89*(A6), 3762–3774, doi:10.1029/JA089iA06p03762.

Viñas, A. F., H. K. Wong, and A. J. Klimas (2000), Generation of electron suprathermal tails in the upper solar atmosphere: Implications for coronal heating, *Astrophys. J.*, *528*(1), 509, doi:10.1086/308151.

Voitenko, Y., and J. De Keyser (2011), Turbulent spectra and spectral kinks in the transition range from MHD to kinetic Alfvén turbulence, *Nonlin. Processes Geophys.*, *18*(5), 587–597, doi:10.5194/npg-18-587-2011.

Voitenko, Y., and M. Goossens (2006), Energization of plasma species by intermittent kinetic Alfvén waves, *Space Sci. Rev.*, *122*(1–4), 255–270, doi:10.1007/s11214-006-8212-0.

Voitenko, Y. M. (1998a), Three-wave coupling and parametric decay of kinetic Alfvén waves, *J. Plasma Phys.*, *60*, 497–514.

Voitenko, Y. M. (1998b), Three-wave coupling and weak turbulence of kinetic Alfvén waves, *J, Plasma Phys.*, *60*, 515–527.

Wygant, J., et al. (2013), The electric field and waves instruments on the radiation belt storm probes mission, *Space Sci. Rev.*, *179*, 183–220, doi:10.1007/s11214-013-0013-7.

Wygant, J. R., A. Keiling, C. A. Cattell, R. L. Lysak, M. Temerin, F. S. Mozer, C. A. Kletzing, J. D. Scudder, V. Streltsov, W. Lotko, and C. T. Russell (2002), Evidence for kinetic Alfvén waves and parallel electron energization at 4–6 R_E altitudes in the plasma sheet boundary layer, *J. Geophys. Res.*, *107*(A8), 1201, doi:10.1029/2001JA900113.

Young, D. T., S. Perraut, A. Roux, C. de Villedary, R. Gendrin, A. Korth, G. Kremser, and D. Jones (1981), Wave-particle interactions near Ω_{He+} observed on GEOS 1 and 2 1. Propagation of ion cyclotron waves in He^+-rich plasma, *J. Geophys. Res.*, *86*(A8), 6755–6772, doi:10.1029/JA086iA08p06755.

Zhang, J.-C., L. M. Kistler, C. G. Mouikis, M. W. Dunlop, B. Klecker, and J.-A. Sauvaud (2010), A case study of EMIC wave-associated He^+ energization in the outer magnetosphere: Cluster and Double Star 1 observations, *J. Geophys. Res.*, *115*, A06212, doi:10.1029/2009JA014784.